

# Coarsening dynamics of ternary amphiphilic fluids and the self-assembly of the gyroid and sponge mesophases: Lattice-Boltzmann simulations

Nérido González-Segredo\* and Peter V. Coveney†

Centre for Computational Science, Department of Chemistry, University College London, 20 Gordon Street,  
London WC1H 0AJ, United Kingdom

(Received 30 October 2003; published 1 June 2004)

By means of a three-dimensional amphiphilic lattice-Boltzmann model with short-range interactions for the description of ternary amphiphilic fluids, we study how the phase separation kinetics of a symmetric binary immiscible fluid is altered by the presence of the amphiphilic species. We find that a gradual increase in amphiphile concentration slows down domain growth, initially from algebraic to logarithmic temporal dependence, and, at higher concentrations, from logarithmic to stretched-exponential form. In growth-arrested stretched-exponential regimes, at late times we observe the self-assembly of sponge mesophases and gyroid liquid-crystalline cubic mesophases, hence confirming that (a) amphiphile-amphiphile interactions need not be long-ranged in order for periodically modulated structures to arise in a dynamics of competing interactions, and (b) a chemically specific model of the amphiphile is not required for the self-assembly of cubic mesophases, contradicting claims in the literature. We also observe a structural order-disorder transition between sponge and gyroid phases driven by amphiphile concentration alone or, independently, by the amphiphile-amphiphile and the amphiphile-binary fluid coupling parameters. For the growth-arrested mesophases, we also observe temporal oscillations in the structure function at all length scales; most of the wave numbers show slow decay, and long-term stationarity or growth for the others. We ascribe this behavior to a combination of complex amphiphile dynamics leading to Marangoni flows.

DOI: 10.1103/PhysRevE.69.061501

PACS number(s): 61.30.St, 61.20.Lc, 64.75.+g

## I. INTRODUCTION

The term *amphiphilic fluid* is broadly used to denote multiphase fluids in which at least one species is of a surfactant nature. A surfactant molecule (from *surface active agent*, which we shall also refer to as an amphiphile) contains a polar headgroup attached to a hydrocarbon tail which, dispersed in a binary immiscible fluid mixture, such as oil and water, is driven towards and adsorbed at the interface between the two fluids. The selective chemical affinity between each part of the surfactant molecule and the components of the binary mixture is the mechanism responsible for such a taxis [1]. Not only are amphiphilic fluids important in physical chemistry, structural biology, soft matter physics, and materials science from a fundamental perspective, but their applications are also widespread. Detergents and mammalian respiration are two common examples in which surfactants are present. Living cell membranes are complex macromolecular assemblies comprised in large part of self-assembled phospholipids, of an amphiphilic nature [2]. Sponge mesophases are formed as a result of an amphiphile dispersion or melt at an appropriate composition, and enjoy numerous applications in medical research as well as the pharmaceutical, cosmetic, food, and agrochemical and petrochemical industries [3,4]. Liquid-crystalline bicontinuous cubic mesophases of monoglycerides and the lipid extract from

archaeobacterium *Sulfolobus solfataricus* have been found at physiological conditions in cell organelles and physiological transient processes such as membrane budding, cell permeation, and the digestion of fats [5]. Amphiphilic cubic mesophases can also be synthesised for important applications in membrane protein crystallization, controlled drug release, and biosensors [6,7]. These phases are termed *mesophases* not only because their intrinsic internal length scales range between those characteristic of molecular and hydrodynamic (or macroscopic) realms, but also their mechanical properties are halfway between those found in a liquid and a solid [1,2,8].

Amphiphiles have the property of lowering the interfacial tension in a binary immiscible, say oil-water, fluid [8]. Given the bipolar nature of their molecular structure, amphiphile adsorption at the oil-water interface is a process which is energetically favored relative to their entropically beneficial dispersion in the bulk. This effectively reduces the pressure tensor at the interface, making the immiscible species more alike. As more interfacial surface is created, so more amphiphile dispersed in the bulk can be accommodated at it.

The effect of adding surfactant above a critical concentration to an oil-water mixture undergoing phase separation is to slow down the demixing process, which, with the addition of sufficient amphiphile, can be totally arrested. Langevin, molecular dynamics, and lattice-gas simulations have shown that, as the concentration of dispersed surfactant increases, the temporal growth law of the average size of the immiscible oil-water domains, of the power-law form  $t^a$  in the surfactantless case [9,10], is seen to cross over to a slower, logarithmic growth of the form  $(\ln t)^\theta$ , where  $a$  and  $\theta$  are fitting parameters and  $t$  is the time [11–13]. Emerton *et al.*

\*Also at Department de Física, Universitat Autònoma de Barcelona, 08193 Bellaterra, Barcelona, Spain. Email address: n.gonzalez-segredo@ucl.ac.uk

†Email address: p.v.coveney@ucl.ac.uk

showed that increasing the surfactant concentration even further leads to growth well described by the stretched exponential  $A-B \exp(-Ct^D)$ , where  $A$ ,  $B$ ,  $C$ , and  $D$  are fitting parameters, including halted segregation at sufficiently late times [13]. Depending on temperature, pressure, and fluid composition in such a stretched exponential regime, the amphiphile can self-assemble and force the oil-water mixture into a wealth of equilibrium structures. The self-assembling process is dictated by the competing attraction-repulsion mechanisms present among the species. Lamellae and hexagonally packed cylinders are examples of these mesophases, also referred to as  $L_\alpha$  and  $H$ , respectively, with continuous translational symmetry along one or two directions. Other examples are the sponge ( $L_3$ ) mesophase and the micellar ( $Q^{223}$  or  $Pm3n$ , and  $Q^{227}$  or  $Fd3m$ ), primitive (“ $P$ ”,  $Q^{229}$ , or  $Im3m$ ), diamond (“ $D$ ”, “ $F$ ”,  $Q^{224}$ , or  $Pn3m$ ), and gyroid (“ $G$ ”,  $Q^{230}$ , or  $Ia\bar{3}d$ ) cubic mesophases, all of which lack continuous translational symmetry [14]. Among all the aforementioned phases, only the sponge mesophase is devoid of long-range order and so cannot be classified as a liquid crystal: it is rather characterized by glassy features.

A sponge mesophase formed by the amphiphilic stabilization of a phase-segregating binary fluid mixture is called a microemulsion. Since we shall be dealing with oil and water in equal proportions, we shall be concerned with bicontinuous microemulsions. A bicontinuous microemulsion is a structure consisting of two percolating, interpenetrating oil and water phases separated by a monolayer of surfactant molecules adsorbed at the interface. Oil and water are isotropically mixed, and ordering is short range. Sponge phases formed by the dispersion of amphiphile in a single-phase solvent differ from microemulsions in that it is a surfactant bilayer which underlies the structure, and the regions it divides are occupied by the same fluid component. A gyroid phase is also a bicontinuous, interpenetrating structure; however, ordering is evidently long range, whence its classification as a liquid crystal. In the gyroid, the locus where most of the surfactant resides is a triply periodic minimal surface (TPMS) whose unit cell is of cubic symmetry. The surface has zero mean curvature, no two points on it are connected by a straight segment, and no reflexion symmetries are present. Isosurfaces of the gyroid phase for which oil and water are not at equal composition (minority phases) form mutually percolating, threefold coordinated, regular lattices. Other examples of triply periodic surfaces of zero mean curvature arise in the  $P$  and  $D$  mesophases, the minority-phase isosurfaces of which exhibit coordination numbers of six and four, respectively.

The purpose of the present paper is to report on a theoretical study of the segregation kinetics in ternary amphiphilic fluids and the self-assembly of the sponge and gyroid mesophases. By progressively adding surfactant to an initially homogeneous immiscible oil-water mixture on the way to achieving arrested domain growth, we shall give an account of how the segregation kinetics of the fluid domains is affected by the addition of surfactant, and study the features of the associated mesophases that are formed. The mesophases corresponding to such late time, arrested growth regimes are sponges which turn into gyroids as we increase

the surfactant concentration. We shall also see that these phases exhibit temporal oscillations in the size of the oil-water domains, which we ascribe to Marangoni flows.

## II. OVERVIEW OF MODELING AND SIMULATION OF AMPHIPHILIC FLUID SELF-ASSEMBLY

Various methods have been used to date to model and simulate ternary amphiphilic mixtures and to study their phase-segregation kinetics and the formation of microemulsions and liquid-crystalline phases. We briefly review them in this section.

Kawakatsu *et al.* studied segregation kinetics employing a two-dimensional hybrid model with thermal noise but without hydrodynamics, combining a continuum, Langevin diffusion equation for the oil-water dynamics and Newtonian dynamics with dissipation for bipolar particles modeling the surfactant [11]. They used a free energy in the form of a  $\phi^4$ -Ginzburg-Landau expansion [15] plus terms modeling the surfactant-interface and surfactant-surfactant interactions. They found the average domain size of symmetric binary immiscible fluids with amphiphile to grow with time more slowly than  $t^{1/3}$ , the latter expected for binary alloys in two and three dimensions. Laradji *et al.*, instead of modeling the amphiphile as a particulate species, regarded it as a continuous density coupled to the oil-water order parameter in a  $\phi^4$ -Ginzburg-Landau free energy [12]. In their work, they studied several cases of two-dimensional Langevin diffusion equations, one of which being the so-called Model  $D$  [16]. Model  $D$  incorporates noise, a conserved order parameter, and surfactant density, but excludes hydrodynamics. Laradji *et al.* not only found logarithmic growth for the behavior of the average domain size with time, but also observed a slow-down from it for higher surfactant concentrations and dynamical scaling for the structure function at intermediate times. Yao and Laradji, using a modified Lifshitz-Slyozov nucleation theory for continuum fields in two and three dimensions, studied how the Ostwald ripening dynamics of an asymmetric mixture of oil and water is altered by the presence of a surfactant species [17]. They found results similar to those of Laradji *et al.* [12].

The segregation kinetics of amphiphilic fluids have also been studied with fully particulate methods such as classical molecular dynamics and, more recently, hydrodynamic lattice gases. Using a minimalist molecular dynamics model in two dimensions, Laradji *et al.* [18] found a crossover scaling function similar to previous Langevin [11] and Lifshitz-Slyozov models [17], yet with a different algebraic exponent, and a slowing down from the algebraic growth laws for binary mixtures. Using two-dimensional hydrodynamic lattice-gas models for symmetric [13] and asymmetric mixtures [19], the group of Coveney found that surfactant induces a crossover to a logarithmic slow growth, and, with sufficient surfactant, full arrest of domain growth which is well described by a stretched exponential function. The group found similar results with a three-dimensional hydrodynamic lattice-gas model [20].

Particulate methods have also been used to tackle mesophase self-assembly. Using classical molecular dynamics

methods, Marrink *et al.* simulated evolution of a surfactant bilayer, initially set up on the morphology of a “*D*” TPMS, to study both the surfactant packing structure and how close such a bilayer would remain to the TPMS after relaxation [6]. They, however, did not address self-assembly dynamics: time scales required for that are orders of magnitude above those reachable with atomistic techniques on present-day cutting-edge supercomputers. In dissipative particle dynamics (DPD) approaches, a Langevin dynamics with momentum conservation is solved to model ill-defined, mesoscopic dissipative particles interacting via repulsive, soft potentials; hydrodynamics is emergent and the amphiphile is represented by dissipative particles bound together by rods or springs [21–23]. The DPD simulations of Groot and Madden of copolymer melts [21] showed that melts of symmetric amphiphile led to lamellar phases, whereas a gyroidlike structure appeared only for asymmetric amphiphile as a transient phase, precursor to a hexagonally packed tubular phase. Nekovee and Coveney, using the lattice-Boltzmann model we employ in this work, were able to reproduce the “*P*” mesophase in a binary amphiphilic mixture of surfactant and solvent [24].

Many of the simulation studies on the formation kinetics of microemulsion and liquid-crystalline mesophases have made use of stochastic Langevin diffusion methods, in which mass currents are driven by chemical potential gradients computed from free energies of the ubiquitous  $\phi^4$ -Ginzburg-Landau expansion form. These models treat the amphiphile only implicitly through the functional dependence of the surface tension parameter with the amphiphile density [25–29]. In cases in which the amphiphile is a copolymer, however, the free energy is often derived from polymer models which aim at accounting for the amphiphile’s molecular structure with a certain degree of specificity [30–32]. The validity of these Flory-Huggins-type approaches rests on being able to derive the free energy from a microscopic model, which not only might entail considerable difficulty but does require the segregation to be a quasistatic, local equilibrium process. Under general far from equilibrium conditions, such as occurs in the sudden-quench scenario so often employed in the literature, equilibrium thermodynamic potentials are known not to adequately describe the process. Besides, free-energy-based methods also require surfactant adsorption and relaxation on the interface to be much faster than interface motion, a so-called *adiabatic approximation*. Free-energy approaches are frequently represented as paradigms of thermodynamically consistent mesoscopic methods; some of them also pursue chemical specificity in elaborate empirical exercises amounting to little more than parameter fitting of polymer models. The philosophy behind them, nonetheless, is the use of macroscopic, local equilibrium information to specify a stochastic, and hence mesoscopic, nonequilibrium dynamics. None of these methods offers a dynamics satisfying detailed balance, let alone an *H* theorem (Lyapunov function) guaranteeing irreversible evolution towards the equilibrium state described by the prescribed free energy. As a consequence, the “thermodynamic consistency” of these methods remains on shaky grounds.

The fact that some free-energy approaches [31,32] focus on the specific molecular structure of the amphiphile raises

the question of what use particulate methods, such as is the one we report in this paper, have in the simulation of amphiphilic fluid systems. Our method, by reducing the description of the amphiphilic molecule to its minimal possible expression—a point dipole,—retains the minimum number of degrees of freedom necessary to model interfacial adsorption and micellization, and, additionally, in a hydrodynamically consistent framework which does not require processes to be quasistatic. With these basic properties at our disposal, we want to fully exploit our model’s capabilities to determine the nonequilibrium amphiphilic dynamics and the equilibrium fluid structures arising from it. The minimalistic bottom-up approach is in line with the fact that, far enough from criticality, distinct molecular structures and microscopic dynamics can produce similar macroscopic behavior—this is universality emerging from microscopic complexity [33]. In addition, particulate methods are much more suitable than conventional continuum fluid dynamics methods [34] for the simulation of interface dynamics. Such dynamics is an emergent property of the underlying interparticle interactions among the immiscible species; a set of continuum partial differential equations describing the locus of the interface is, rather, its macroscopic manifestation, and its solution a much more laborious endeavor. *A fortiori*, modeling surfactant adsorption and self-assembly in an explicit fashion via particulate methods provides a more realistic picture of the microscopics than doing so at the continuum, macroscopic limit described by free-energy approaches.

Lattice-Boltzmann (LB) methods were originally developed as a means of reducing the computational cost associated with lattice-gas automation (LGA) algorithms [35]. LB methods evolve a single-particle distribution function via a discretized Boltzmann equation, usually in the linearized, relaxation-time (BGK) approximation. Such a single-particle distribution, at a particular time slice and spatial position on the lattice, is an average over the LGA velocity space for a statistically large number of different microscopic realizations (initial conditions). The fact that much of the phenomenology of binary immiscible and ternary amphiphilic fluids occurs for small spatiotemporal gradients permits us to take the mean-field (or molecular chaos) approximation, and the Boltzmann-Grad limit in which such an approximation holds, as heuristically appropriate for the modeling of their universal properties. Heuristics come into play in that tunable parameters are introduced in LB models in order to reproduce desired quantities of dense and/or complex fluids, such as surface tension, viscosity, and thermal conductivity (for required values of Reynolds and Prandtl numbers), stress tensors (for required viscous or viscoelastic behavior), and equations of state (for liquid-gas and phase-segregating transitions). It is worth noting that the increasing popularity of LB methods in recent years is primarily based on pragmatic considerations associated with their simplicity and algorithmic efficiency.

This paper presents the first quantitative account of amphiphilic phase-segregation dynamics using a three-dimensional model based on the Boltzmann transport equation. It describes the spontaneous self-assembly of the gyroid liquid-crystalline cubic mesophase and an order-disorder transition between the latter and the sponge mesophase, of

glassy features. The remainder of the paper is structured as follows. In Sec. III we describe the model. In Sec. IV we look at how the segregation kinetics of the fluid domains is affected by the addition of surfactant. Section V studies the temporal oscillations of the average domain size and the structure function, which are only observed for segregation-halted regimes. In Sec. VI we characterize the morphology of the mesophases corresponding to those regimes via direct- and Fourier-space imaging, and identify the sponge $\leftrightarrow$ gyroid structural transition. Finally, we provide conclusions in Sec. VII.

### III. A LATTICE-BOLTZMANN MODEL FOR TERNARY AMPHIPHILIC FLUIDS

The amphiphilic lattice-Boltzmann model we employ in this paper is derived from that originally proposed by Chen *et al.* [36,37]. The method can be regarded as a fully mesoscopic, bottom-up approach, which does not require the existence of a thermodynamic potential describing phase transitions. In fact, the method is athermal in the sense that, for algorithmic efficiency reasons, the microdynamics is devised *ex professo* to conserve velocity moments of the distribution function only up to first order; this simplification is valid wherever fluctuations are negligible, e.g., away from criticality. This is, for example, the case of deep quenches into the spinodal region of the fluid's phase diagram, which is our case in this paper. As opposed to top-down LB methods, based on the imposition of a free-energy functional [38,39], the global dynamics arise as an emergent property of the interactions between mesoscopic levels of description, in agreement with a complexity paradigm [33]. Oil-water segregation is achieved via interspecies forces which modify the fluid's macroscopic velocity. The dynamics in the bulk of each binary immiscible species (e.g., oil and water) can be derived from a Boltzmann equation with a forcing term. An amphiphilic molecule is modeled as a continuously orientable massive point dipole subjected to thermal noise and relaxing towards an equilibrium that minimizes its interaction energy with mean fields generated by its nearest neighbors on the lattice. The densities of surfactant, oil, and water evolve via coupled lattice-BGK equations. This is a mean-field approach which exhibits Galilean invariance and reproduces correct hydrodynamics. We have also shown, in a previous paper which serves as a reference benchmark for this study [9], that the model reproduces the dynamical scaling hypothesis during the phase segregation experienced by binary immiscible (oil-water) fluids. Its algorithmic simplicity allows it to achieve extremely high performance on massively parallel computers [40], and substantially reduces the domain of numerical instability present in free-energy-based LB methods [9]. Because an  $H$  theorem is lacking in essentially all multiphase lattice-Boltzmann models hitherto proposed [41], we consider it artificial to try to enforce a prescribed thermodynamic equilibrium in these schemes; a method which is algorithmically simpler, fully mesoscopic, mean-field and bottom-up is of greater fundamental interest.

#### A. Binary immiscible fluids

The core of our model is a lattice-BGK equation governing the evolution of the mass density distribution  $m^\alpha n_k^\alpha(\mathbf{x}, t)$

of component  $\alpha$  in an interacting fluid mixture at position  $\mathbf{x}$ , instant  $t$ , and for discrete molecular velocity  $\mathbf{c}_k$ , on a regular lattice and in discrete time. Here,  $m^\alpha$  is the particle mass which we set to unity for convenience, and the single-particle distribution  $n_k^\alpha(\mathbf{x}, t)$  obeys the lattice-BGK relaxation-streaming mechanism:

$$n_k^\alpha(\mathbf{x} + \mathbf{c}_k, t + 1) - n_k^\alpha(\mathbf{x}, t) = \Omega_k^\alpha, \quad (1)$$

where the collision term has two contributions accounting for the kinetics of noninteracting (ideal) plus interacting (nonideal) multicomponent species, respectively:

$$\Omega_k^\alpha(\mathbf{x}, t) \equiv \Omega_k^{(0)\alpha}(\mathbf{x}, t) + \sum_{\bar{\alpha}} \sum_l \Lambda_{kl}^{\alpha\bar{\alpha}} n_l^{\bar{\alpha}}, \quad (2)$$

the sums extending over all available species and directions, and

$$\Omega_k^{(0)\alpha}(\mathbf{x}, t) \equiv - \frac{n_k^\alpha(\mathbf{x}, t) - n_k^{\alpha(\text{eq})}(\mathbf{x}, t)}{\tau^\alpha}. \quad (3)$$

Here, the time increment and lattice spacing are both unity,  $\mathbf{x}$  is a node of such a lattice,  $\alpha = r, b$  [e.g. oil ( $r$ ) or water ( $b$ )], and  $\mathbf{c}_k$  is one of the 24 ( $\equiv N_{\text{vec}}$ ) discrete velocity vectors plus one null velocity of the projected face centered hypercubic D4Q25 lattice we use to guarantee isotropy in the macroscopic equations that the model reproduces for a bulk, single-phase fluid [42]. The parameter  $\tau^\alpha$  defines a velocity-independent relaxation rate towards equilibrium for component  $\alpha$ ;  $\Lambda_{kl}^{\alpha\bar{\alpha}}$  can be regarded as a matrix element of a cross-collision operator  $\Lambda$  which is a function of both  $\tau^\alpha$  and the acceleration  $\mathbf{a}^\alpha$ , the latter being experienced by a fluid element due to its neighbors, as will be defined later. The function  $n_k^{\alpha(\text{eq})}(\mathbf{x}, t)$  in Eq. (3) is the discretization of a third-order expansion in Mach number of a local Maxwellian [9], representing the local equilibrium state of the  $\alpha$ th component,

$$n_k^{\alpha(\text{eq})}(\mathbf{x}, t) = \omega_k n^\alpha(\mathbf{x}, t) \left[ 1 + \frac{1}{c_s^2} \mathbf{c}_k \cdot \mathbf{u} + \frac{1}{2c_s^4} (\mathbf{c}_k \cdot \mathbf{u})^2 - \frac{1}{2c_s^2} u^2 + \frac{1}{6c_s^6} (\mathbf{c}_k \cdot \mathbf{u})^3 - \frac{1}{2c_s^4} u^2 (\mathbf{c}_k \cdot \mathbf{u}) \right], \quad (4)$$

where  $\omega_k$  are the coefficients resulting from the velocity space discretization, and  $c_s$  is the speed of sound, both of which are determined by the choice of the lattice. For the projected D4Q25 lattice we use, the speed of sound is  $c_s = 1/\sqrt{3}$ ,  $\omega_k \equiv 1/3$  for the speed  $c_k = 0$ , and  $1/36$  for speeds  $c_k = 1$  and  $\sqrt{2}$ . In Eq. (4),  $\mathbf{u} = \mathbf{u}(\mathbf{x}, t)$  is the macroscopic velocity of the mixture, through which the collision term couples the different molecular velocities  $\mathbf{c}_k$ . This is because  $\mathbf{u}$  is a function of the components' macroscopic velocities, defined as  $n^\alpha(\mathbf{x}, t) \mathbf{u}^\alpha \equiv \sum_k n_k^\alpha(\mathbf{x}, t) \mathbf{c}_k$ .

A judicious choice of the coefficients in the expansion of the equilibrium distribution Eq. (4), allows for mass and momentum to be (nonlocally) conserved for the noninteracting, ideal gas mixture case, i.e.,

$$\sum_k \Omega_k^{(0)\alpha} = 0, \quad \sum_\alpha m_\alpha \sum_k \mathbf{c}_k \Omega_k^{(0)\alpha} = 0. \quad (5)$$

It can be shown that in the limit of creeping flows to second order, i.e.,  $u^2 \approx 0$ , the expression for the fluid mixture's macroscopic velocity  $\mathbf{u}$  required for momentum conservation in the absence of interactions, as a function of  $\mathbf{u}^\alpha$ , simplifies to that obtained for a second-order expansion of the equilibrium distribution, namely  $\mathbf{u} \equiv \sum_\alpha (\rho^\alpha \mathbf{u}^\alpha / \tau^\alpha) / \sum_\alpha (\rho^\alpha / \tau^\alpha)$ , which we have incorporated in our implementation.

The form of the collision term (2) derives from adding an increment  $\Delta \mathbf{u}^\alpha$  to the fluid mixture's macroscopic velocity  $\mathbf{u}$  which enters in the equilibrium distribution (4), i.e.,  $\Omega_k^\alpha(\mathbf{u}) \equiv \Omega_k^{(0)\alpha}(\mathbf{u} + \Delta \mathbf{u}^\alpha)$  where  $\Delta \mathbf{u}^\alpha \equiv \mathbf{a}^\alpha \tau^\alpha$  and  $\mathbf{a}^\alpha \equiv \mathbf{F}^\alpha / \rho^\alpha$ . Here

$$\mathbf{F}^{\alpha,c}(\mathbf{x}, t) \equiv -\psi^\alpha(\mathbf{x}, t) \sum_{\bar{\alpha}} g_{\alpha\bar{\alpha}} \sum_{\mathbf{x}'} \psi^{\bar{\alpha}}(\mathbf{x}', t) (\mathbf{x}' - \mathbf{x}) \quad (6)$$

is the mean-field force density felt by phase  $\alpha$  at site  $\mathbf{x}$  and time  $t$  due to its surroundings;  $g_{\alpha\bar{\alpha}}$  is a coupling matrix controlling the interfacial tension between the fluid species, interface adsorption/desorption properties of the surfactant molecules, and the surfactant-surfactant interaction;  $\psi^\alpha$  is an *effective mass* which serves as a functional parameter and can have a variety of forms for modeling various types of fluids. We only allow nearest-neighbor interactions,  $\mathbf{x}' \equiv \mathbf{x} + \mathbf{c}_k$ , and choose  $\psi^\alpha(\mathbf{x}, t) \equiv 1 - \exp[-n^\alpha(\mathbf{x}, t)]$ , where  $n^\alpha \equiv \sum_k n_k^\alpha$ . This choice for  $\psi$  has also been made by Shan and Chen to model liquid-gas phase transitions [43] although, as we shall see, our motivation here is different.

### B. Amphiphilic fluids

The incorporation of a third, amphiphilic species not only requires the inclusion of an extra label ("s") for the superscript denoting the species in Eq. (1), but also a modification of the cross-collision operator  $\Lambda$  since amphiphiles interact with fluid elements and between themselves. In addition, the physics of amphiphilic molecules, namely, self-assembly and adsorption to immiscible fluid interfaces, cannot be modeled without introducing a new type of body force: in Sec. III A ordinary bulk fluid species are thought of as pointlike particles given that their interactions depend on their relative distances alone. For surfactant molecules, however, their orientations are important too [36], and a dipole is the simplest configuration to mimic their essential character. In short, we must extend the scalar lattice-BGK model hitherto described into a vector model.

Each surfactant molecule is represented by an average dipole vector  $\mathbf{d}(\mathbf{x}, t)$  at each site and time step, whose orientation is allowed to vary continuously. The average is taken over nearest neighbors before advection, according to the propagation equation

$$n^s(\mathbf{x}, t+1) \mathbf{d}(\mathbf{x}, t+1) = \sum_k \tilde{n}_k^s(\mathbf{x} - \mathbf{c}_k, t) \tilde{\mathbf{d}}(\mathbf{x} - \mathbf{c}_k, t), \quad (7)$$

where the tildes denote postcollisional values, as defined by Eq. (1) for the  $\Lambda \equiv 0$  ( $g_{\alpha\bar{\alpha}} \equiv 0$ ) case if we replace the leftmost summand with  $\tilde{n}_k^\alpha(\mathbf{x}, t)$ . For the sake of simplicity and computational efficiency, the model does not assign microscopic

velocities  $\mathbf{c}_k$  to single-dipole vectors but to site-averaged surfactant densities instead, as can be seen, for example on the right-hand side of Eq. (7).

Dipole relaxation is governed by the BGK process

$$\tilde{\mathbf{d}}(\mathbf{x}, t) = \mathbf{d}(\mathbf{x}, t) - \frac{1}{\tau^s} [\mathbf{d}(\mathbf{x}, t) - \mathbf{d}^{\text{eq}}(\mathbf{x}, t)], \quad (8)$$

where  $\tau^s$  is a new parameter controlling the relaxation towards the local equilibrium  $\mathbf{d}^{\text{eq}}(\mathbf{x}, t)$ , which is understood as the average orientation with respect to the Gibbs measure, i.e.,

$$\mathbf{d}^{\text{eq}}(\mathbf{x}, t) \equiv d_0 \frac{\int d^2\Omega e^{-\beta H_{\hat{\Omega}}(\mathbf{x}, t)} \hat{\Omega}}{\int d^2\Omega e^{-\beta H_{\hat{\Omega}}(\mathbf{x}, t)}}, \quad (9)$$

where  $d^2\Omega$  is an element of solid angle whose director is the unit vector  $\hat{\Omega}$  representing the dipole orientation, and  $\beta$  is an inverse temperaturelike parameter. The modulus of the left-hand side of Eq. (9) ranges between 0 and the scale value  $d_0$ , chosen to be unity for convenience. That, along with  $\tau^s \geq 1$ , guarantees the magnitude of the dipole vector to be less than  $d_0$  at all times. Equation (9) favors surfactant orientations which minimize the *energy*  $H_{\hat{\Omega}} \equiv -\hat{\Omega} \cdot \mathbf{h}(\mathbf{x}, t)$ , where  $\mathbf{h}(\mathbf{x}, t)$  is the sum of the mean fields created by surrounding bulk fluid and surfactant, namely,

$$\mathbf{h}^c(\mathbf{x}, t) \equiv \sum_\alpha q_\alpha \sum_k n^\alpha(\mathbf{x} + \mathbf{c}_k, t) \mathbf{c}_k, \quad (10)$$

$$\mathbf{h}^s(\mathbf{x}, t) \equiv \sum_k \left[ n_k^s(\mathbf{x}, t) \mathbf{d}(\mathbf{x}, t) + \sum_{l \neq 0} n^s(\mathbf{x} + \mathbf{c}_l, t) \theta_l \cdot \mathbf{d}(\mathbf{x} + \mathbf{c}_l, t) \right] \quad (11)$$

allowing for nearest-neighbor interactions only. The first equation is a discrete approximation to the color gradient for the immiscible species, where  $q_\alpha = 0, \pm 1$  is the color charge of species  $\alpha$ . The second equation is a dipole vector density, where summation over  $k$  performs local dipole averaging, summation over  $l$  includes all nearest-neighbor contributions, and the second-rank tensor  $\theta_l \equiv \mathbf{I} - D \mathbf{c}_l \mathbf{c}_l / c^2$ , where  $c$  is the modulus of  $\mathbf{c}_l$  and  $D$  is the spatial dimension, picks up desired orientations from nearest-neighbor dipoles. Finally, Eq. (9) can be integrated analytically in three dimensions to give  $\mathbf{d}^{\text{eq}} = d_0 [\coth(\beta h) - 1 / \beta h] \hat{\mathbf{h}}$ , where  $h$  is the magnitude of  $\mathbf{h}$  and  $\hat{\mathbf{h}}$  its unit vector.

The new interactions that modify the interspecies collision operator  $\Lambda$  are the force on an immiscible fluid element from other fluid elements and amphiphiles,  $\mathbf{F}^\alpha \equiv g_{\text{br}} \mathbf{F}^{\alpha,c} + g_{\text{bs}} \mathbf{F}^{\alpha,s}$ , where  $\mathbf{F}^{\alpha,c}$  is that in Eq. (6), and the force on an amphiphilic molecule from neighboring fluid elements and amphiphiles,  $\mathbf{F}^s \equiv g_{\text{bs}} \mathbf{F}^{s,c} + g_{\text{ss}} \mathbf{F}^{s,s}$ . In these expressions,  $g_{\text{br}}$ ,  $g_{\text{bs}}$ , and  $g_{\text{ss}}$  are coupling scalar parameters, and the analytical expressions for each force term, derived in Ref. [36], are

$$\mathbf{F}^{\alpha,s} \equiv -2g_{\alpha s} \psi^\alpha(\mathbf{x}, t) \sum_{k \neq 0} \tilde{\mathbf{d}}(\mathbf{x} + \mathbf{c}_k, t) \theta_l \cdot \psi^s(\mathbf{x} + \mathbf{c}_k, t), \quad (12)$$

$$\mathbf{F}^{s,c} \equiv 2\psi^s(\mathbf{x},t)\tilde{\mathbf{d}}(\mathbf{x}+\mathbf{c}_l,t) \cdot \sum_{\alpha} g_{\alpha s} \sum_{k \neq 0} \theta_k \psi^{\alpha}(\mathbf{x}+\mathbf{c}_k,t), \quad (13)$$

$$\begin{aligned} \mathbf{F}^{s,s} \equiv & -\frac{4D}{c^2} g_{ss} \psi^s(\mathbf{x},t) \sum_k \{ \tilde{\mathbf{d}}(\mathbf{x}+\mathbf{c}_k,t) \cdot \theta_k \cdot \tilde{\mathbf{d}}(\mathbf{x},t) \mathbf{c}_k \\ & + [ \tilde{\mathbf{d}}(\mathbf{x}+\mathbf{c}_k,t) \tilde{\mathbf{d}}(\mathbf{x},t) + \tilde{\mathbf{d}}(\mathbf{x},t) \tilde{\mathbf{d}}(\mathbf{x}+\mathbf{c}_k,t) ] \cdot \mathbf{c}_k \} \\ & \times \psi^s(\mathbf{x}+\mathbf{c}_k,t). \end{aligned} \quad (14)$$

Equations (12)–(14) were derived considering only nearest-neighbor interactions, modeling each dipole as a dumbbell of oppositely color-charged particles displaced  $\pm \mathbf{d}/2$  from the dipole's center of mass location  $\mathbf{x}$ , and carrying out Taylor expansions of the force (6) to leading order in  $\mathbf{d}$  about  $\mathbf{x}$  as well as those at the neighboring sites [36]. Also, Eq. (13) is the reaction to force (12), and Taylor expansions in the ratio of  $|\mathbf{c}_k|$  to the length scale that the color gradient sets can be used to further simplify the expressions. Finally, additional coupling parameters  $g_{\alpha\bar{\alpha}}$  have been introduced, where  $g_{ss}$  should be chosen negative to model attraction between two amphiphile heads or tails, and repulsion between a head and a tail.

### C. Selection of the parameters for the simulations

The model is implemented as a parallel code in FORTRAN90 making use of the message passing interface parallel paradigm [44] and spatial domain decomposition, and incorporating wrap-around, periodical boundary conditions in all three dimensions. It was executed on 16 to 64 processors on SGI Origin2000 and Origin3800 parallel platforms. The form  $\psi \equiv 1 - \exp[-n(\mathbf{x},t)]$  for the effective mass in the force in Eq. (6) was heuristically chosen so as to broaden the region of numerical stability in parameter space: numerical instabilities can arise as the result of high values of forces and speeds, and are more likely to occur in our model when surfactant interactions are included than for binary immiscible fluids [9,45].

Preliminary studies allowed us to determine the values of the model's various parameters for which an initially thorough mixture of two immiscible fluid phases plus a dispersed amphiphilic species produced a segregated mixture with arrested domain growth [45]. Those values were the surfactant thermal parameter  $\beta=10.0$ , all particle masses and relaxation times set to 1.0, and coupling constants  $g_{br}=0.08$ ,  $g_{bs}=-0.006$ , and  $g_{ss}=-0.003$ . [Masses  $m^{\alpha}$  enter in the description through  $\rho^{\alpha}(\mathbf{x},t) \equiv \sum_k m^{\alpha} n_k^{\alpha}(\mathbf{x},t)$ .] We simulated the behavior of a ternary mixture by varying the coupling constants around the values mentioned above, and for initial surfactant particle densities ranging in the interval  $0.00 \leq n^{(0)s} \leq 0.90$ . The lattice sites and directions were initially populated with flatly distributed mass densities,  $0 \leq \rho_k^{\alpha}(\mathbf{x},0) \leq m^{\alpha} n^{(0)\alpha} / N_{\text{vec}}$ , where  $n^{(0)\alpha}$  is the particle density of phase  $\alpha$ , and  $k$  numbers each of the  $N_{\text{vec}}=24$  velocity vectors. We determined that setting  $n^{(0)\alpha} > 0.6$  for both species guaranteed immiscibility. In all the simulations we present here we set oil:water mass

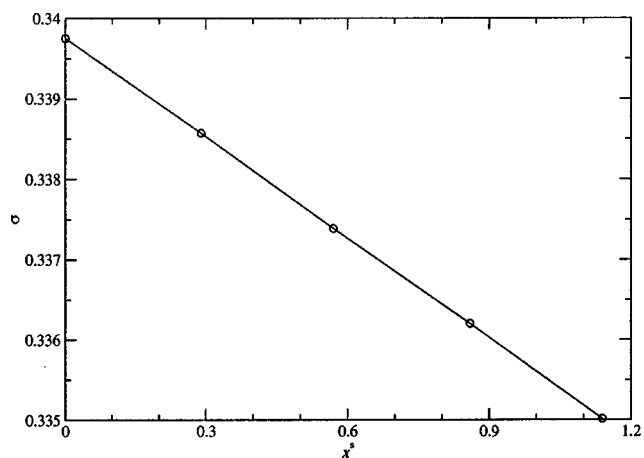


FIG. 1. Surface tension dependence on the surfactant concentration (mass fraction, cf. Table I) as measured at a planar interface making use of Eq. (15). A lattice of size  $4 \times 4 \times 128$  was allowed to evolve up to time step 25 000, and pressure tensor components were measured every 1000 time steps. The surface tension tends to grow with time and reaches a horizontal asymptote; at that time step the surface tension only differs in 16 % from that at the previous measurement. Interpolation serves as a reference to the eye. Coupling constants used were  $g_{br}=0.08$ ,  $g_{bs}=-0.006$ , and  $g_{ss}=-0.003$ . Oil and water densities used were  $n^{(0)R}=n^{(0)B}=0.7$ . All quantities are reported in lattice units.

fractions to 1:1, specifically at  $n^{(0)\alpha}=0.7$  for  $\alpha=r,b$ .

It is experimentally known that the addition of amphiphile into an immiscible fluid mixture reduces the interfacial tension, as has also been reported for various lattice-gas models in two and three dimensions [13,20]. To confirm that our model reproduces this important property, we ran simulations on a  $4 \times 4 \times 128$  lattice of a planar interface with surfactant adsorbed onto it and whose initial density was varied between simulation runs. The surface tension was calculated with the line integral along the normal to the interface [46],

$$\sigma = \int_{-\infty}^{+\infty} [P_{zz}(z) - P_{xx}(z)] dz, \quad (15)$$

where, for the pressure tensor  $\mathbf{P} \equiv \{P_{ij}\}$ , we used the expression [9]

$$\begin{aligned} \mathbf{P}(\mathbf{x}) = & \sum_{\alpha} \sum_k \rho_k^{\alpha}(\mathbf{x}) \mathbf{c}_k \mathbf{c}_k + \frac{1}{4} \sum_{\alpha, \bar{\alpha}} g_{\alpha\bar{\alpha}} \sum_{\mathbf{x}'} [ \psi^{\alpha}(\mathbf{x}) \psi^{\bar{\alpha}}(\mathbf{x}') \\ & + \psi^{\bar{\alpha}}(\mathbf{x}) \psi^{\alpha}(\mathbf{x}') ] (\mathbf{x} - \mathbf{x}') (\mathbf{x} - \mathbf{x}'). \end{aligned} \quad (16)$$

We restrict ourselves in this study to nearest-neighbor interactions,  $\mathbf{x}' \equiv \mathbf{x} + \mathbf{c}_k$ , and transversal symmetry allows the second summand within the integrand in Eq. (15), which in general is  $\frac{1}{2}(P_{xx}+P_{yy})$ , to be simplified as shown. Equation (16) contains a kinetic (first) term, the momentum flux, due to the free streaming of particles corresponding to an ideal gas contribution, plus a potential or virial (second) term due to the interparticle momentum transfer derived from the force (6) [47,48].

Figure 1 shows the surface tension  $\sigma$  plotted against ini-

TABLE I. Surfactant densities employed in the study of the algebraic-to-logarithmic and logarithmic-to-stretched exponential transitions. The mass fraction  $x^s$  is the ratio of  $n^{(0)s}$  to  $n^{(0)b} = n^{(0)r} = 0.7$ , and the rest of the parameters used were  $g_{br} = 0.08$ ,  $g_{bs} = -0.006$ ,  $g_{ss} = -0.003$ , masses and relaxation times set to 1.0, and  $\beta = 10.0$ . The lattice used was sized  $64^3$  for all simulation runs except 01, for which it was  $128^3$  in order to avoid finite size effects entering at about  $L \approx 25$ .

Simulation run	01	02	03	04	05	06	07	08
$n^{(0)s}$	0.0	0.15	0.22	0.30	0.35	0.40	0.60	0.90
$x^s$	0.0	0.21	0.31	0.43	0.50	0.57	0.86	1.3

tial surfactant density, and details on parameters and densities used are included in the caption. Notice that in the regime the binary fluid is in, and for the values of surfactant density we use, the surface tension decreases linearly with surfactant concentration. It is entirely possible that there may be departures from linearity were we to increase the surfactant concentration beyond that shown in Fig. 1 because of interfacial saturation with surfactant, as observed in two- and three-dimensional lattice-gas studies [13,20].

#### IV. DOMAIN GROWTH KINETICS

We ran simulations starting with a homogeneous mixture of oil and water particle mixture to which surfactant was randomly added across on the lattice. Lattice sizes employed were  $64^3$  and  $128^3$  to assess finite size effects. Each lattice site was populated with a density uniformly distributed in the range zero up to the values summarized in Table I.

The average size of the oil-water domains is a natural measure of the degree of segregation within the mixture. We define it as the inverse first moment of the spherically averaged oil-water structure function,  $L(t) \equiv 2\pi/k_1(t)$ , where  $k_1(t) \equiv \sum_k k S(k, t) / \sum_k S(k, t)$ . The spherically averaged oil-water structure function  $S(k, t)$  is  $\sum_{\hat{\mathbf{k}}} \hat{k} S(\mathbf{k}, t) / \sum_{\hat{\mathbf{k}}} 1$ , where the  $S(\mathbf{k}, t)$  is the oil-water structure function,

$$S(\mathbf{k}, t) \equiv \frac{\mathfrak{s}}{V} |\phi'_{\mathbf{k}}(t)|^2, \quad (17)$$

and  $\sum_{\hat{\mathbf{k}}}$  denotes summation over the set of wave vectors contained in the spherical shell  $n - \frac{1}{2} \leq (V^{1/3}(k/2\pi) \leq n + 1/2$ , for integer  $n$ . Equation (17) is the Fourier transform of the spatial autocorrelation function for the oil-water order parameter  $\phi \equiv \rho^r - \rho^b$ , where  $V$  is the lattice volume,  $\mathfrak{s}$  is the volume of the lattice unit cell, and  $\phi'_{\mathbf{k}}(t)$  is the Fourier transform of the fluctuations of the order parameter,  $\phi$ . Our choice of the structure function, rather than alternative measures of domain size such as the autocorrelation function, was made on the basis that it is directly proportional to x-ray or neutron scattering intensities, hence facilitating direct comparison with empirical data [49].

In Fig. 2 we plot the temporal evolution of the average domain size  $L$  for the surfactant concentrations of Table I. The amount of surfactant needed to slow down the kinetics of the binary immiscible oil-water mixture (simulation run

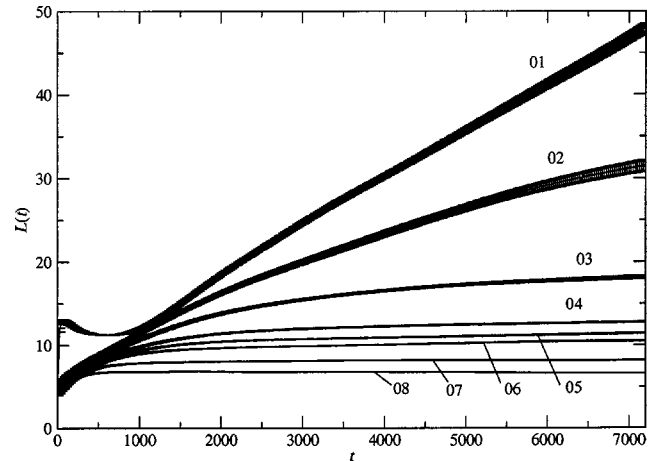


FIG. 2. Temporal evolution of the average fluid-fluid domain size for surfactant concentrations 0.0, 0.15, 0.22, 0.30, 0.35, 0.40, 0.60, and 0.90 for curves from top to bottom and corresponding to simulation runs 01, 02, 03, 04, 05, 06, 07, and 08, respectively (cf. Table I). Measurements have been taken every 25 time steps, and the plots include error bars, which represent the uncertainty (one standard error) transmitted from the standard error of the structure function spherical average. We used a lattice of size  $128^3$  for simulation run 01 and  $64^3$  for the remaining curves, since finite size effects start to creep in for domain sizes larger than  $L \approx 30$ . All quantities are reported in lattice units. Note that the surfactant-containing fluids lack the zero-growth, linear transient found for simulation run 01 [11].

01) is seen to be relatively low. We now need to find the growth laws that best fit these data. Previous simulation studies, for 1:1 oil-water fluid mixtures with or without surfactant [9,13,20,37], have found algebraic, logarithmically slow and stretched exponential behaviors, given as

$$a_1(t - b_1)^{c_1}, \quad (18)$$

$$a_2(\ln t)^{c_2}, \quad (19)$$

$$a_3 - b_3 \exp[-c_3(t - d_3)^{e_3}], \quad (20)$$

to be those characterizing the temporal growth of the average domain size,  $L(t)$ , of an oil-water mixture without surfactant, Eq. (18) [9], and when surfactant is added above a minimum threshold concentration, Eq. (19), and at a sufficiently high amphiphile concentration, Eq. (20), the latter being a regime for which arrested growth is reached at late times. The coefficients  $a_i$  and  $b_i$  ( $i = 1, 2, 3$ ) are fitting parameters. While we shall take these functional forms as suggested choices, we would also like to find out how closely they in fact fit our data.

Linearity in the  $(t, L)$  data cloud on a log-log plot would permit us to ascertain whether or not the data follow Eq. (18), regardless of the zero-time offset value  $b_1$  since this is a horizontal displacement. To find out which data may be better fit by Eq. (19), we would require  $(\ln t, L)$  pairs of data in a search for linearity on a log-log plot. This method, however, is not likely to be of much help given the small differ-

ence between plots of the logarithm of a data series and plots of the logarithm of such logarithmic data, as we shall see. We therefore prefer to adopt the criterion of considering candidates for the model of Eq. (18) from the log-log linearity method, while resorting to both visual inspection and a search for a reduced chi-squared statistic ( $\chi^2/\text{ndf}$ ) close to 1.0 in order to identify a slower growth such as that of Eq. (19) (ndf is the number of degrees of freedom). Finally, Eq. (20) possesses a distinctive horizontal asymptote which best fits data whose domain growth at late times is fully arrested.

From the linearity of curves in Fig. 3 we can infer that simulation runs 01 and 02 (Table I) are good candidates for the growth model of Eq. (18). Figure 3, however, leads to the same conclusion, as expected given the small difference between these two plots. We then resort to looking at the  $\chi^2/\text{ndf}$  statistic in assessing how well Eqs. (18) and (19) fit simulation runs 01, 02, and 03, see Table II. The binary immiscible fluid simulation run 01, with no surfactant present, exhibits an exponent consistent with the system being in a crossover between the known diffusive ( $t^{1/3}$ ) and viscous hydrodynamic ( $t^{1.0}$ ) regimes, already reported for binary immiscible fluids simulated with the lattice-BGK model we employ in this paper [9]. Simulation run 02 has the peculiarity that Eq. (18) holds (poorly) only during an initial transient, and Eq. (19) takes over to give a very good fit at later times,  $t > 1100$ . This transient is due to the time required by the surfactant to adsorb onto the interface and affect the binary immiscible interfacial dynamics. Finally, simulation run 03 is best fit by Eq. (19), although the high  $\chi^2/\text{ndf}$  value indicates that the data contain more detail than the model does. In addition, from Fig. 3(b), this mixture segregates at a slower speed than that given by Eq. (19), yet it does not reach total arrest, at least up to 7200 time steps. Rather, total arrest is seen at higher surfactant concentrations, as in runs 06 and 07 (see Fig. 6). We conclude that simulation run 03 represents a fluid which is in a transition regime between the logarithmic and the stretched exponential behaviors. A similar behavior was previously observed by others using lattice-gas methods in two [13] and three dimensions [20], and lattice-Boltzmann methods in two dimensions [37]. Emerton *et al.*, using a two-dimensional lattice-gas model, reported the divergence of the coefficients of Eq. (20) in an attempt to fit data for which total growth arrest had not been achieved [13]. The fits to our data, which include error bars, also produced the same divergences. Their fluid mixtures as well as ours, we conclude, were, rather, in a transitional regime well described by a growth law slower than Eq. (19) which still allowed for domain growth. It is, however, possible that growth arrest could be achieved at later times; this prearrest regime would then be a long-lived transient.

We now look at wave numbers of the spherically averaged structure function  $S(k)$  other than the first moment, already provided by  $L(t)$ . Figure 4 shows the spherically averaged structure function for simulation run 06 at several time steps. The temporal evolution of the curves resembles the segregation kinetics for binary immiscible fluid mixtures, except that domain growth arrest for late times makes them tend to superimpose. Note that a hump appears at these times, indicat-

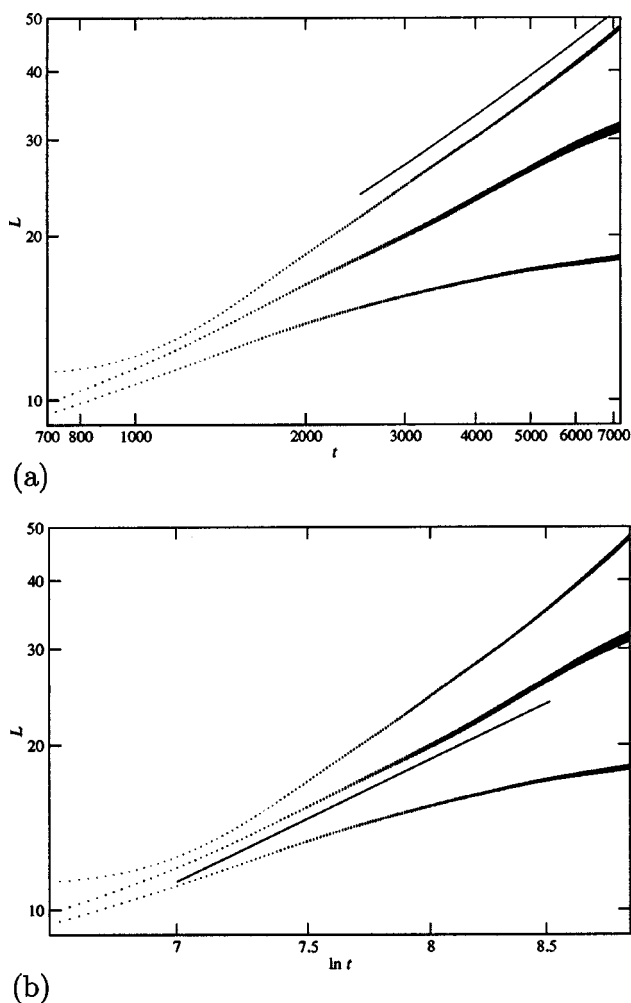


FIG. 3. Panel (a) shows the time evolution of the average domain size for simulation runs 01, 02, and 03, see Fig. 2. The log-log scale helps to visually detect behaviors following Eq. (18)—in this case, that of the uppermost curve. The straight line above it serves as a guide to the eye only and its slope is given by  $c_1$  in Table II. Panel (b) shows the evolution of the average domain size with the logarithm of the time step for simulation runs 01, 02, and 03, on a log-log scale. This is useful to discriminate growth between that of Eqs. (18) and (19); see Table II for the fitting parameters. The straight solid line shown indicates a good fit to Eq. (19) for  $t > 1100$  ( $\ln t \approx 7$ ). For  $t < 1100$ , the curve is better fit by Eq. (18), albeit still quite poorly. Measurements have been taken every 25 time steps, and the plot includes error bars representing the uncertainty (one standard deviation) of the spherical averaged structure function. We use a  $128^3$  lattice for simulation run 01 and a  $64^3$  lattice for the remainder. All quantities are reported in lattice units.

ing the formation of structures, statistically weak, of size close to half the lattice side length. Inspection of  $\phi(\mathbf{x})$  snapshots suggests the spurious presence of elongated domains of such sizes which are extended rather than folded. At the late times we examined, these elongations tend to vanish or fold. Still in Fig. 4, it is worth noting that for all length scales above a threshold (about  $k < 0.9$ ), curve superposition is not sharp. This is a consequence of the fact that for the fluid composition of simulation run 06, and those of higher sur-

TABLE II. Fits of the average domain size growth with time to the models of Eqs. (18) and (19) for simulation runs corresponding to surfactant mass fractions 0.0, 0.21, and 0.31, from top to bottom, respectively, as detailed in Table I. Lattice sizes used were  $128^3$  for simulation run 01 and  $64^3$  for the rest. Poor fits are indicated as blank fields. Simulation run 02 shows two behaviors in its temporal evolution, Eq. (18) for  $t < 1100$  and Eq. (19) for  $t > 1100$ . Note the very good value of the  $\chi^2/\text{ndf}$  statistic for the latter. The poor value of the statistic for simulation run 03 indicates that Eq. (19) is insufficient and a more detailed model is required, albeit not Eq. (20).

Simulation run	$c_1$	$\chi^2/\text{ndf}$	$c_2$	$\chi^2/\text{ndf}$
01	$0.896 \pm 0.007$	0.18		
02	$0.644 \pm 0.004$	7.5	$3.850 \pm 0.010$	0.92
03			$2.649 \pm 0.022$	39

factant concentrations, there are small temporal oscillations in  $S(k)$ . All these mixtures have in common that they have achieved total growth arrest—in fact,  $L(t)$  decreases in time for simulation run 08, as we shall see later on and discuss in more detail. Oscillations in the structure function and a hump at low wave numbers have been reported previously in a hydrodynamic Langevin model of sponge phase dynamics, using field-theoretic methods [28]. However, this approach did not consider the amphiphile concentration explicitly but, rather, embedded it into a Ginzburg-Landau free energy through the surface tension, in a scenario where amphiphile relaxation is assumed to be fast compared to that of the oil-water order parameter.

In Figs. 5(a) and 5(b) we show the spherically averaged structure function at time step 7200 of the mixtures in Table

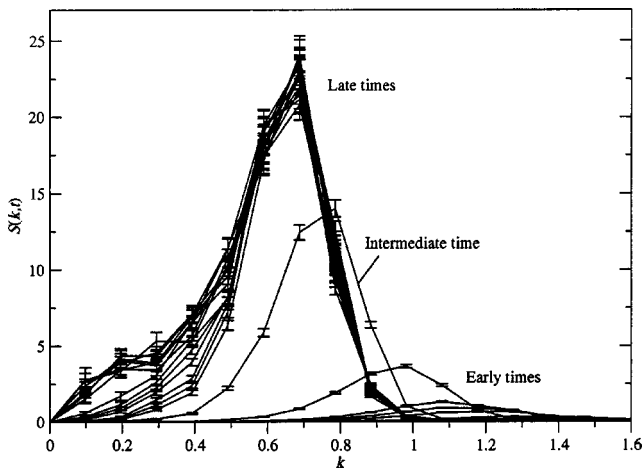


FIG. 4. Spherically averaged structure functions for the oil-water order parameter simulation run 06 (cf. Table III). According to how close to asymptotic behavior the distribution of domain sizes appears to be, we have classified simulation times for this simulation run in three groups: early times (time steps 25, 50, 75, 125, 150, 175, and 300 in the plot), intermediate times (time steps roughly from 800 to 1700), and late times (time steps 1800, 2300, 2800, 3300, 3800, 4300, 4800, 6000, 10 000, 14 000, 18 000, 22 000, 26 000, and 30 000 in the plot). Error bars represent the standard error of the shell average. Lattice size is  $64^3$ . All quantities are reported in lattice units.

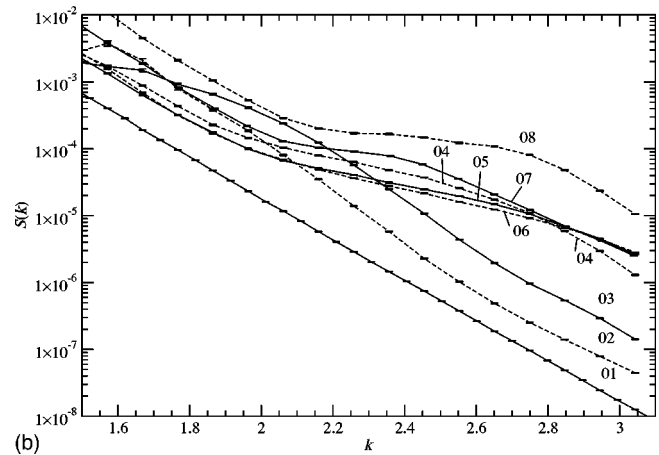
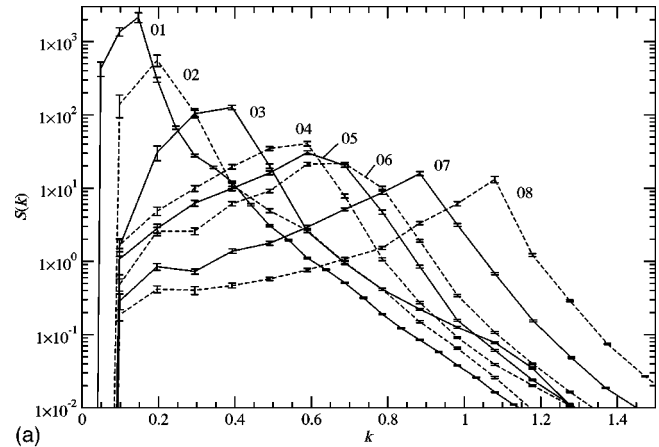


FIG. 5. Log-linear plots of the spherically averaged structure functions at time step 7200 for increasing surfactant concentrations indicated by the numerical labeling on each curve, corresponding to simulation runs 01, 02, 03, 04, 05, 06, 07, and 08, respectively, cf. Table I. For large wavelengths, panel (a), we can see how the peaks move to higher wave numbers, decrease in height, and broaden. Note that for short wavelengths, panel (b), the only straight tail is for curve  $n^{(0)s}=0.0$ , whose slope is  $-4.46 \times 10^{-4}$ . Error bars represent one standard error of the shell average  $S(k)$ . Lattice size is  $128^3$  for simulation run 01 and  $64^3$  for the others. All quantities are reported in lattice units.

I, for the larger and smaller length scales, respectively. As the initial density of surfactant is increased in a series of replica initially homogeneous water-oil-surfactant fluid mixtures, as indicated by Table I, it is expected that the oil-water structure function peaks will move to higher wave numbers, decrease in intensity, and broaden [4,8,50]. This is indeed what we observe in Fig. 5(a). Note that at smaller length scales, Fig. 5(b), the exponential decay of the structure function that occurs for simulation run 01 does not hold for the ternary amphiphilic mixtures. This can be explained by the contribution of small micellar structures that form in the bulk of each immiscible phase, more likely to take place for mixtures of higher surfactant concentration. Indeed, in Fig. 5(b), the latter exhibit the most manifest deviations.

TABLE III. Parameters employed in studying domain size oscillations, whose onset occurs for surfactant mass fractions  $x^s \geq 0.57$ ; the remaining parameters of the model are stated in the caption of Table I, also for the additional runs 09 and 10, in lattice units.

Simulation run	$n^{(0)s}$	$x^s$	$g_{ss}$	$g_{bs}$
06	0.40	0.57	-0.0030	-0.006
07	0.60	0.86	-0.0030	-0.006
08	0.90	1.3	-0.0030	-0.006
09	0.60	0.86	-0.0045	-0.006
10	0.60	0.86	-0.0030	-0.009

### V. SELF-SUSTAINED OSCILLATIONS

Arrest of domain growth occurs for high surfactant density only, cf. Fig. 2, as expected. Further inspection, however, shows that not only are there small temporal oscillations of the average domain size, as we mentioned at the end of the last section, but also that they do not die out during the simulation window. Similarly to what was previously reported using a bottom-up lattice-Boltzmann method in two dimensions akin to the one employed here [37], the amplitude of the oscillations is very small compared to the average domain size, and smaller than previous lattice-gas simulations in two and three dimensions [13,20]. The fact that, in lattice-gas methods, these oscillations persist after ensemble averaging is consistent with their occurrence in lattice-Boltzmann approaches, since the latter are effectively ensemble-averaged versions of the former. Since the systems we simulate are dissipative and isolated (there is no mass or momentum exchange with external sources), oscillations, however, are expected to die out at sufficiently late times.

Motivated by the observation of oscillating average domain sizes, we performed additional simulation runs in order to check the role of the coupling constants  $g_{ss}$  and  $g_{bs}$  in the reproduction of such oscillations, our hypothesis being that both an increased surfactant-surfactant interaction and an increased tendency for surfactant to adsorb on the interface might be expected to have an influence on their frequency and amplitude. In Table III we summarize the parameters used in the new simulation runs (09 and 10) along with those of previous oscillating fluid mixtures.

Figure 6 shows the temporal oscillations in the average domain size for the mixtures of Table III, and Fig. 7 shows their structure functions at time step 17 000. All these mixtures exhibit domain growth arrest; interestingly, Fig. 6 shows that the average domain size shrinks in time for some of them (mixtures 08 and 09). In addition, we uncover the role that the coupling constants  $g_{ss}$  and  $g_{bs}$  have in the oscillations: while increasing  $|g_{ss}|$  seems to enhance their frequency, an increase in  $|g_{bs}|$  drastically dampens them and reduces their amplitude. However damped the oscillations of simulation run 10 may seem, zooming into smaller scales reveals the existence of minute oscillations (less than 0.10 lattice sites in amplitude), which is not the case for simulation runs 01 through to 05. (Note that the length scales reported in Fig. 6 are lattice averages; an amplitude being less

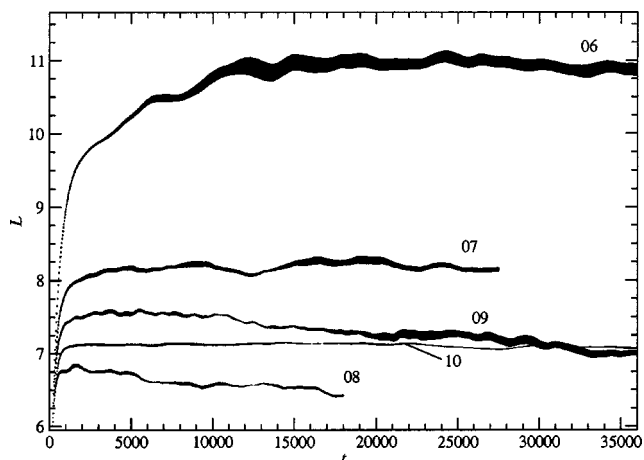


FIG. 6. Temporal evolution of the average domain size for simulation runs 06, 07, 09, 10, and 08, as seen from top to bottom at  $t = 10\,000$  (cf. Table III). Measurements have been taken every 25 time steps; error bars are included and represent the uncertainty (“one sigma”) transmitted from the standard error of the spherically averaged structure function. *Caveat lector*: an oscillation in the average domain size is genuinely representative of oscillations in the domain sizes only if error bars are smaller than the oscillation amplitude. Lattice size is  $64^3$ . All quantities are reported in lattice units.

than one lattice site hence remains physically meaningful.) Oscillations are, therefore, the signature of all growth-halted regimes.

The structure function plots of Fig. 7 provide further insight into the role of coupling constants  $g_{ss}$  and  $g_{bs}$  in the oscillation dynamics. Note that mixture 08 produces a peak of intensity similar to that of mixture 07, a feature already seen at much earlier times [see Fig. 5(a)]. This peak height similarity could have been ascribed to a transient, such as turned out to be the case for the difference in peak intensities between mixtures 06 and 07; however, it persisted in time. Mixture 09 also shows a peak intensity similar to that of

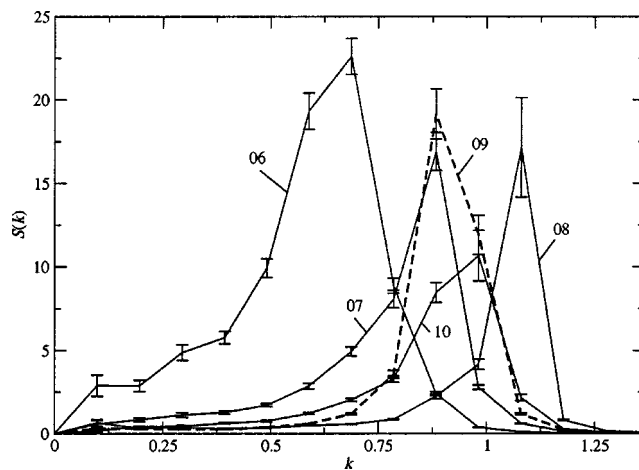


FIG. 7. Structure functions at late time step 17 000 for simulation runs 06, 07, 09, 10, and 08 (cf. Table III). Error bars represent the standard error of the shell average  $S(k)$ . Lattice size is  $64^3$ . All quantities are reported in lattice units.

mixture 07. Peak intensities bear a direct relation to the steepness of oil-water domain walls and, hence, to their surface tension. The fact that increasing the surfactant concentration (in mixture 08 compared to mixture 07) does not reduce the surface tension denotes that the interface is close to its saturation limit with respect to surfactant adsorption. If enough surfactant is dispersed in the bulk, a process of diffusion towards and adsorption onto the interface could continue to occur, much slower compared to the initial adsorption leading to growth arrest, which could explain the slow domain size reduction. In the cases of simulation runs 08 and 09, close to interface saturation, surfactant concentration in the bulk is high. An amphiphilic mixture being close to the saturation limit implies that the value of its surface tension is the lowest among all amphiphilic mixtures sharing the same composition, relaxation times and coupling constants  $g_{\alpha\bar{\alpha}}$ . Surface tension may be further reduced only by allowing more surfactant molecules onto the interface, which can be done by increasing  $|g_{bs}|$ . This is exactly what we observe in Fig. 7 for fluid composition 10.

As we saw in Fig. 4, small oscillations in the average domain size indicate that the structure function varies in time back and forth between distributions of sizes which are close to each other. The first moment of such distributions, as studied in Fig. 6, may not be representative of the dynamics at other length scales, as we shall see immediately. In Fig. 8 we show the temporal evolution of  $S(k)$  for mixture 09 for a range of wavelengths. Note three characteristic features of the  $S(k)$  curves: they all oscillate, decrease for  $k < 0.785$  and  $k > 1.08$ , and increase or remain stationary in the long time average for  $k \approx 0.884$  and  $k \approx 0.982$ . This behavior corresponds to the sharpening of the distribution  $S(k)$  with time. Modes with  $k > 1.28$  ( $L < 4.91$ ) decay fast enough [ $S(k) < 0.1$  for  $t \approx 1000$ ] for them to be negligible in terms of their contribution to the fluid mesostructure. Other decreasing modes take much longer ( $t > 30\,000$ ) to vanish.

Our study of the oscillations would be incomplete without looking at frequency power spectra. The time series we analyze correspond to  $S(k=0.589)$  of fluids 06, 07, 09 and 10; this choice is made on the basis that this wave number apprehends characteristic features of each data set. From each time series we subtracted its longest waves (i.e., its envelope), computed as the average  $(1/\lambda)\sum_{t'} S(k, t')$ ,  $\lambda$  being a lag large enough so as to decouple high-frequency from low-frequency waves ( $\lambda=5000$  time steps), the sum extending over the interval  $t-\lambda/2 \leq t' \leq t+\lambda/2$ . The Fourier transform of the resulting time series we take as the definition of  $S(k, \omega)$ , cf. Fig. 9. Note therein two high peaks for simulation run 06, and a collection of weak peaks (which we define as those whose heights are less than 5% the height of the largest peak) occurring for higher frequencies. An increase in surfactant density (simulation run 07) causes the number of excited high-frequency modes to grow slightly, yet they also decrease in intensity. Simulation run 09, which differs from mixture 07 in having an increased  $|g_{ss}|$ , very clearly exhibits a substantial increment in the number of excited high-frequency modes. Finally, the spectrum for mixture 10 corroborates the quenching effect on fluctuations caused by increasing  $|g_{bs}|$ .

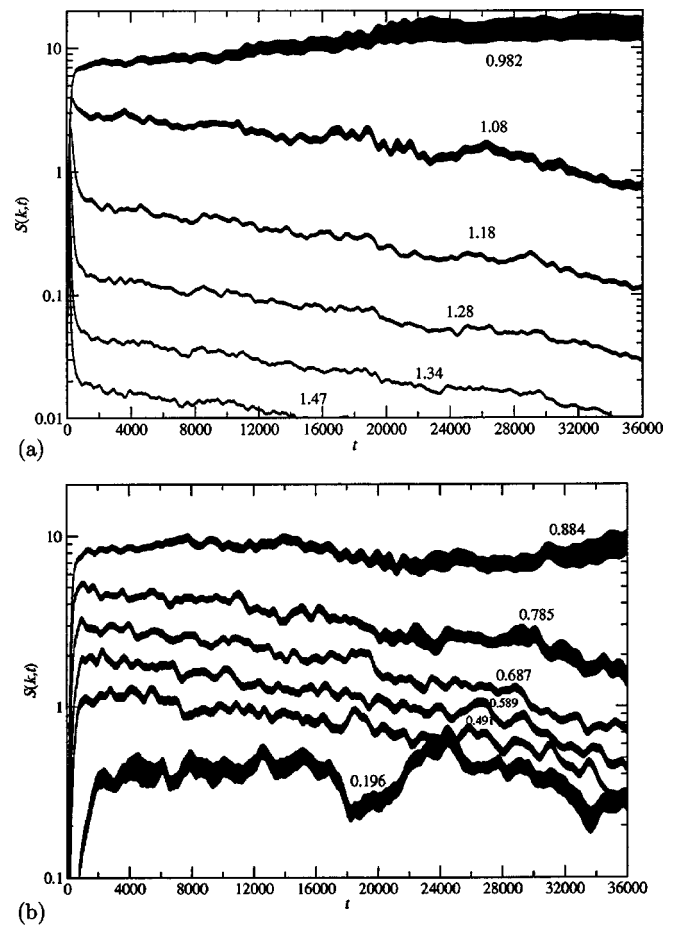


FIG. 8. Temporal dependence of the structure function for simulation run 09, cf. Table III. Panels (a) and (b) show the short and long wavelengths, respectively. Measurements have been taken every 25 time steps; error bars have been included. Lattice size is  $64^3$ . All quantities are reported in lattice units.

The term Marangoni instability describes a convective flow caused wherever an inhomogeneous temperature or mass distribution locally alters the interfacial tension [51]. By visualizing the oil-water interface for mixtures 06 to 10 we observed that the density of adsorbed surfactant is not evenly distributed on it; hence the conditions are set for the appearance of Marangoni instabilities. Figure 10 displays the late-time evolution of a subdomain of a fluid of the same composition as simulation run 09 but simulated on a larger ( $128^3$ ) lattice. We display the surfactant density on a slice through the midplane of the subdomain, along with the locus of the oil-water interface depicted as an isosurface cropped close to the plane. Surfactant inhomogeneities on the interface are evident from these images, as well as the existence of a slow, creeping flow. Distinctive features include the regularity of the order parameter (which we shall study in detail shortly), the existence of high surfactant density necks bridging adjacent portions of the interface, and local regions where regularity is absent, reminiscent of the defects in crystalline materials, which possess their own larger-scale dynamics.

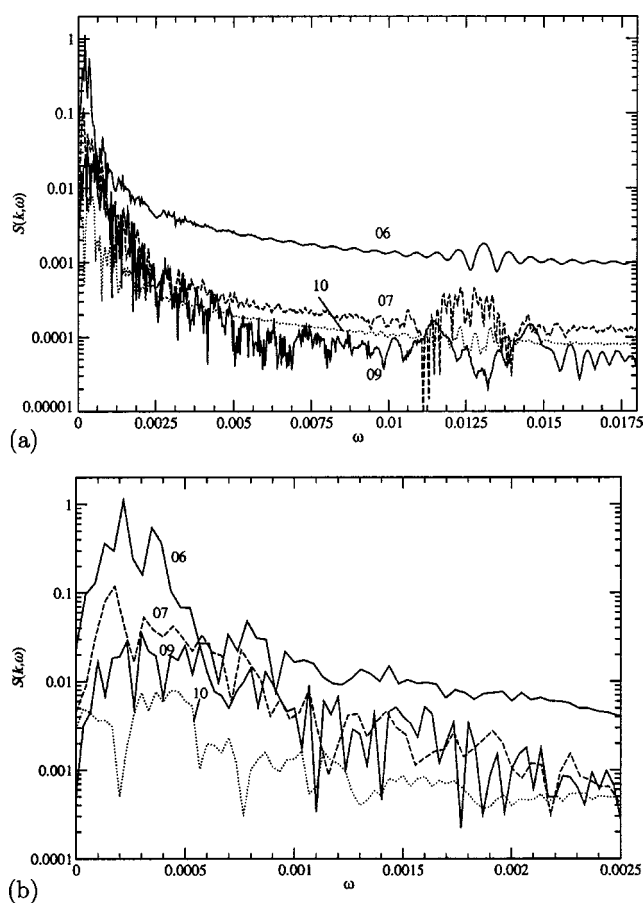


FIG. 9. Frequency power spectra of the structure function for simulation runs 06, 07, 09, and 10 (cf. Table III) at wave number 0.589. Panel (b) is a blowup of panel (a) for long periods of oscillation. Error bars were neither considered for the Fourier analysis nor plotted here. All quantities are reported in lattice units, and  $\omega$  is the inverse period.

## VI. THE SPONGE AND GYROID MESOPHASES

It is known that, in an initially homogeneous 1:1 oil-water mixture, the arrest of phase segregation experienced through the addition of sufficient amphiphile can lead to the formation of a thermodynamically stable bicontinuous sponge phase [11,13,20]. In Fig. 11 we show the late-time morphologies for fluid compositions 06, 07, and 08. They are displayed as the  $\phi(\mathbf{x})=0.37$  isosurface, corresponding to a water-in-oil, “rodlike” scenario, where water is a minority phase and oil is in excess (the order parameter ranges as  $-0.69 \leq \phi \leq 0.68$  over the lattice at that time slice). The structure suggested by minority-phase isosurfaces and the structure of the interface [ $\phi(\mathbf{x})=0$ ] for fluid composition 06 resembles that of a microemulsion, for which structural disorder is the predominant feature. Fluid composition 08, by contrast, shows an evident resemblance to minority-phase images seen in transmission electron microtomography of the gyroid “G” cubic phase [52]. The morphology is an interweaving, chirally symmetric, threefold coordinated, bicontinuous lattice. Fluid mixture 07 seems to be a crossover, *conatus* structure, sharing a substantial amount of disorder with the presence of threefold coordinated “unit cells”; the

latter can be seen as vestigial in fluid system 06. Fluid systems 09 and 10 show that this sponge $\leftrightarrow$ gyroid structural order-disorder transition not only occurs via an increase in surfactant concentration (a lyotropic transition), but in the interaction strength between surfactant with itself and with the interface. We leave for further work a systematic investigation of the  $\{n^{(0)s}, g_{bs}, g_{ss}, g_{br}\}$  parameter space in mapping out the equilibrium mesostructures’ phase diagram. In this endeavor, recently developed *compusteering* tools [53] may prove valuable in optimizing expensive simulation time: they allow the user to postprocess and visualize the compute job’s output at run time with negligible turn-around times, and eventually temporarily stop execution in order to modify simulation parameters which are fed back into the algorithm on immediate restart.

Finite size effects can play an important role in the stabilization of fluidic structures such as these, given that we are using periodic boundary conditions. With this in mind, and using the same parameters as for mixture 09, we computed the wave-number-averaged difference  $\langle \Delta_{N,N'} S \rangle$  for each time step of evolution of the spherically averaged structure function  $S(k)$  between lattices of sizes  $N^3$  and  $N'^3$ , where  $N, N' = 64, 128, 256$ . Note that the lattice size is increased 8 and 64 times from the original  $64^3$  size. Finite size effects would be present if  $\langle \Delta_{N,N'} S \rangle$  were larger than the error derived from the differences and the averages. Nonetheless we found  $\langle \Delta_{N,N'} S \rangle$  to be larger than the error (27% larger on average for  $N=128$  and  $N'=256$ ), the fact that it strongly decreased with  $N$  (i.e.,  $\langle \Delta_{128,256} S \rangle \approx 0.38 \langle \Delta_{64,128} S \rangle$ ) provides the confidence necessary to assert that finite size effects are not significant in the  $N=128$  simulations we are about to report. Moreover, as we shall see immediately, since the structures corresponding to a  $64^3$  lattice exhibit the same morphologies as do the  $128^3$  and  $256^3$  cases, the qualitative features of the former are the same as those for the asymptotic limit  $N \rightarrow \infty$ . This also extends to the oscillation of the structure function: the equivalent of Fig. 8 for the  $128^3$  and  $256^3$  cases (not shown) exhibits similar features, albeit including more wave numbers for which  $S(k)$  grows.

Figure 12 displays three viewpoints of the isosurface  $\phi = 0.40$  for the same composition of fluid mixture 09 as simulated on a  $128^3$  lattice. We show the restriction to a  $33^3$  subdomain, all at time step  $t=15\,000$ , together with the oil-water interface. Whereas on  $64^3$  (or smaller) lattices the liquid-crystalline structure uniformly pervades the simulation cell, on  $128^3$  (and larger) lattices there are some imperfections present resulting in ordered subdomains with slightly varying orientations between which there exist domain boundaries. These boundaries can be considered as defects in the structure, the presence of which is a characteristic feature of liquid crystals. A time scale for the dynamics of some of these defects for our simulated gyroids (simulation run 09) can be roughly estimated from Fig. 10: we observe for that particular slice that the topological genus of the interface changes in an interval ranging between 500 and 1000 time steps. State-of-the-art visualization proved key in the analysis of results, and virtual reality technologies can enhance its usefulness by increasing interactivity with the data.

Small-angle x-ray scattering (SAXS) techniques have been widely used in the determination of the nanostructure of

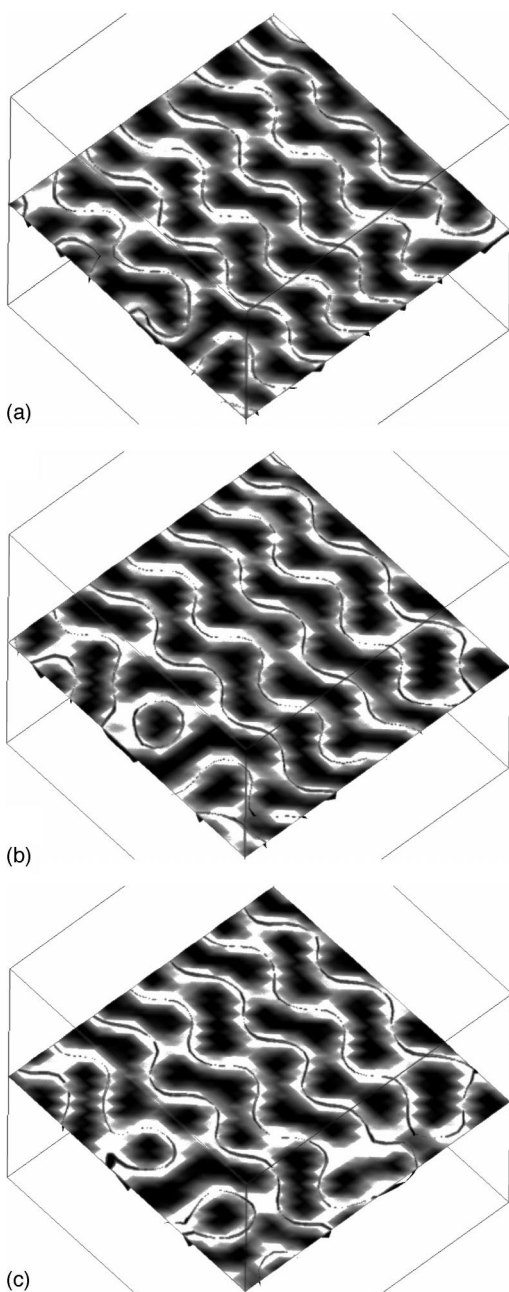


FIG. 10. Slices of the surfactant density in  $33^3$  subsets of a  $128^3$  lattice, for composition 09 (cf. Table I). Panels (a), (b), and (c) are snapshots at  $t=14\,000$ ,  $t=14\,600$ , and  $t=15\,000$  time steps, respectively, which are times for which the structure is close to equilibration. We only show regions where surfactant density is the highest ( $0.31 \leq \rho^s \leq 0.35$ ), in gray and white, where lighter shading denotes a higher value. We can see that the surfactant mainly concentrates around the oil-water interface [ $\phi(\mathbf{x})=0$ ], whose intersection with the slice is depicted as open undulating or closed lines. Also, there are ordered, crystalline regions along with smaller regions lacking long-range order and evolving in time. Finally,  $\rho^s$  is nonuniform on the interface (as regions with lighter shading show), favoring the formation of “surfactant bridges” between adjacent portions of the interface; this leads to Marangoni effects which account for the observed oscillatory behavior. All quantities are in lattice units.

fluid mesophases [14,52,54,55]. SAXS spectra, or their numerically computed versions [56], give peak patterns for these mesophases that are used as fingerprints in determining unknown structures. However, the lattice resolution of our simulations is insufficient to detect multiple peak fingerprints in plots of the spherically averaged structure function. Instead, its unaveraged counterpart  $S(\mathbf{x})$  shows complete agreement of ratios of reciprocal vector moduli with those observed in diffraction patterns of the gyroid, as we display in Fig. 13 for fluid composition 09 [54]. In addition, visual inspection of the unit cell of the oil-water interface unequivocally identifies it with that of the gyroid. The size of such a unit cell as seen in optical textures allows us to associate a length scale to the lattice for a particular experimental realization. For the system reported by Hajduk *et al.* [54], the lattice would need to be 291 nm in side length with a resolution of 2.3 nm per lattice unit.

Although previous simulation papers on amphiphilic mixtures using free-energy-based Langevin diffusion equations have reported the reproduction of structures resembling the gyroid [31,32], none of them have studied its features or dynamics, or incontestably demonstrated its gyroid morphology. Furthermore, in one of these papers we observe that the fluid mesostructure is not stationary [31], whereas by eyeballing the whole simulation cell in another [32] one becomes aware that the structure has a morphology which is reminiscent of the molten gyroid we describe here.

In our simulations we observe that, at late times, the gyroid is much closer to stationarity than the sponge mesophase: for equal time slices in their evolution, temporal changes of the mesostructure over a period of 1000 time steps are considerable for the sponge (e.g., simulation run 06) whereas for the gyroid (e.g., simulation run 09) they appear as slight interfacial rearrangements and undulations, reminiscent of breathing modes, keeping the variation in the position of each unit cell small compared to the lattice size  $N$ . This late-time (ca. 30 000 time steps) structural dynamics is characterized in our simulations by the fact that the topological genus is (statistically) preserved for the gyroid; for the sponge, it is not. This can be understood as structural stabilization by rigidity in the gyroid, and a flowing, glassy dynamics for the sponge. Such a distinctive behavior for the sponge may have a bearing on its density fluctuations and render them different to those occurring in a topology-conserving dynamics. It is therefore not surprising that (a) we found the oscillation modes for the sponge (simulation run 06) to be at least one order of magnitude more intense than those for the different gyroids we simulated (simulation runs 08, 09, and 10, cf. Fig. 9), and (b) recent experimental studies, using dynamic light scattering and various relaxation methods [57], do not report on fluctuations for the gyroid [58], whereas they do for the sponge mesophase.

It is accepted wisdom [59], and a working hypothesis in many simulation studies [25,60,61], that periodically modulated phases may arise in fluid mixtures whenever a repulsive long-range interaction competes with an attractive short-range one for a configuration that minimizes the interfacial Hamiltonian, possibly also in the presence of a thermal, entropic contribution. Little is said about whether nonlocality is not only a sufficient but also a necessary condition, or

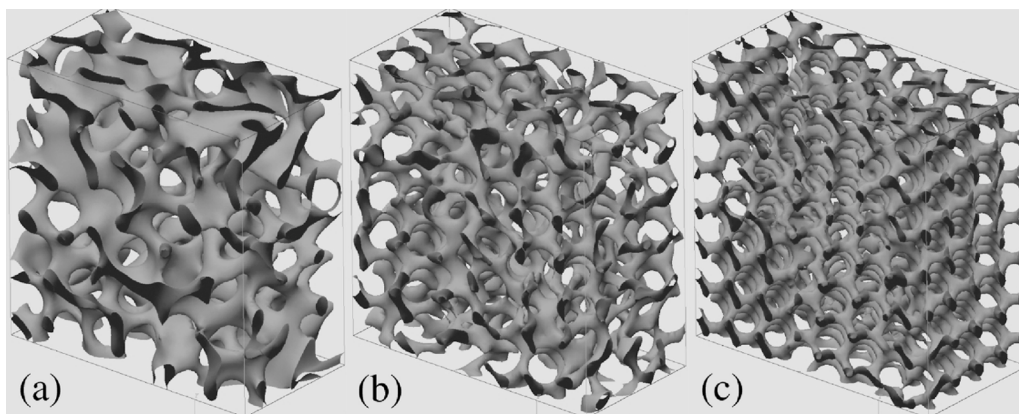


FIG. 11. Equilibrium minority-phase-order parameter isosurfaces  $\phi(\mathbf{x})=0.37$  (in lattice units), taken at time step  $t=30\,000$ , at which  $-0.69 \leq \phi \leq 0.68$  over the whole lattice. Snapshot (a) corresponds to simulation run 06, snapshot (b) to simulation run 07, and snapshot (c) to simulation run 08, cf. Table I. Shown are  $16 \leq z \leq 48$  slabs of a  $64^3$  lattice. Note that increasing surfactant concentration leads to an increased ordering in the mesostructure: simulation run 06 exhibits spongelike features, whereas simulation run 08 is a liquid-crystalline cubic gyroid mesophase. Snapshot (b) is a crossover state in this lyotropic transition—a “molten gyroid.”

whether the nonlocality of the relevant model needs to be imposed *ab initio* or is rather an effective emergent feature picked up by the order-parameter autocorrelation function. The LB model we employ in this paper only incorporates local interactions in its mesodynamics; this feature allows its algorithm to be easily parallelized and achieve exceptionally good performance [40]. Nonetheless, we have demonstrated

that the model is able to simulate liquid-crystalline, cubic mesophases, such as the gyroid in binary immiscible fluid mixtures with an amphiphile, and the primitive “*P*” in binary, amphiphile-solvent mixtures [24], whose density-density correlations are markedly nonlocal, and in the formation of which hydrodynamic interactions play a vital role. Nonlocality, in our case, is an emergent property of a local model.

It is worthwhile pointing out that Prinsen *et al.* [23], using a DPD model and basing their claims on Monte Carlo studies of equilibrium cubic phases by Larson [62], suggested that cubic phases could be engineered to appear if their bead-rod model were elaborated beyond dimers. If fact, Groot and Madden’s (inconclusive) finding of a gyroidlike structure with a DPD model for bead-spring chain copolymers [21] might be considered to support such an assertion. Part of the importance of our simulations, as well as those of Nekovee and Coveney [24], is to refute such conjectures, by demonstrating that cubic mesophases arise in very simple, minimalist, athermal, and hydrodynamically correct fluid models, with a locally interacting vector order parameter and reproducing universal behavior.

### VII. SUMMARY AND CONCLUSIONS

Our simulations furnish the first quantitative account of phase-segregation kinetics and mesophase self-assembly in amphiphilic fluids with a three-dimensional model based on the Boltzmann transport equation. The method is hydrodynamically correct, athermal, and models the amphiphilic species as bipolar, pointlike particles experiencing short-range interactions with mean fields created by the surrounding binary immiscible (“oil-water”) and amphiphilic medium.

We studied the phase-segregation pathway in a homogeneous oil-water-surfactant mixture at composition  $1:1:x$ , respectively, where  $0 \leq x \leq 1.3$  is the surfactant-to-water (or to oil) mass fraction. We observed segregation slowdown in the average size of oil-water domains with increasing  $x$ , and the reproduction of known crossovers, namely, from algebraic to

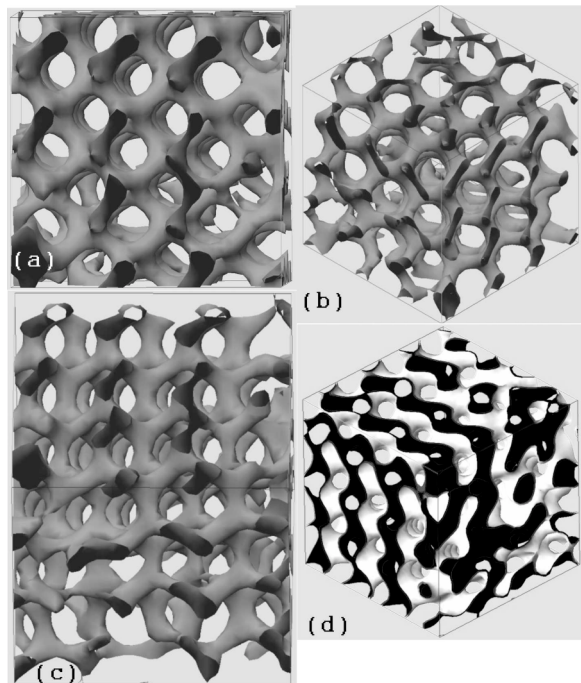


FIG. 12. Isosurfaces of the order parameter at time step  $t=15\,000$  in a highly ordered  $33^3$  subdomain on a  $128^3$  lattice for fluid composition 09. Panels (a), (b), and (c) display the  $\phi(\mathbf{x})=0.40$  (in lattice units) minority-phase isosurface viewed as axonometric projections along the  $(1\,0\,0)$ ,  $(1\,1\,1)$ , and  $(1\,1\,0)$  directions, respectively. Panel (d) shows the interface of the same lattice subdomain along direction  $(1\,1\,1)$ , where black and white have been used to distinguish one immiscible fluid phase from the other.

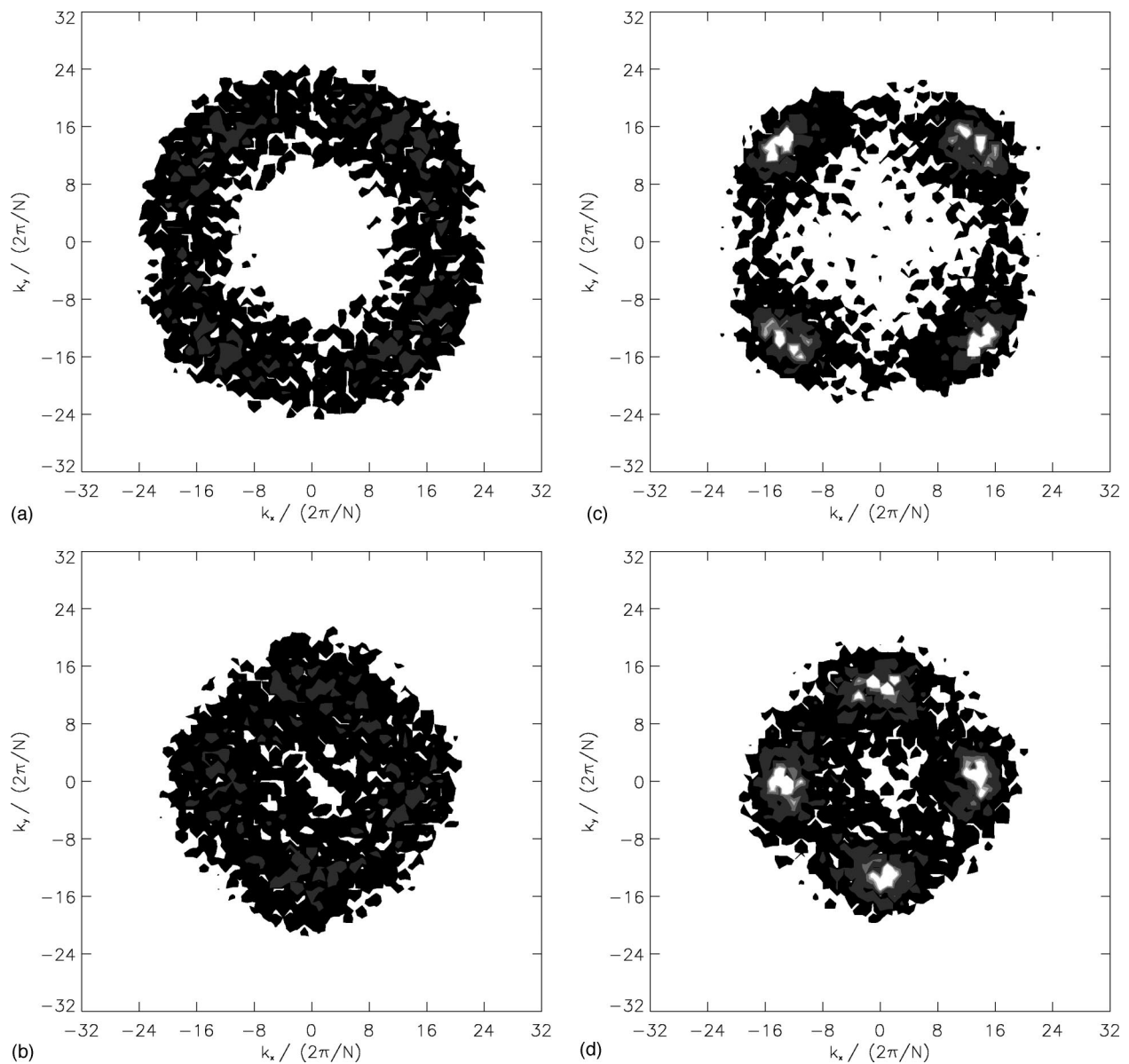


FIG. 13. Temporal evolution of  $(k_x, k_y)$  slices of the structure function  $S(\mathbf{k})$  for fluid composition 09, viewed along the  $(\bar{1}00)$  direction. Panels (a) and (b) show slices at time step  $t=500$ , where  $k_z/(2\pi/N)=0$  for (a) and  $k_z/(2\pi/N)=\pm 14$  for (b). Similarly, panels (c) and (d) are slices at time step  $t=15\,000$  for  $k_z/(2\pi/N)=0, \pm 14$ , respectively;  $N=128$  is the lateral lattice size. Shading denote intensities  $S=1, 50$ , and  $100$ , where lighter grays up to white mean higher intensities. The spherical shell structure in (a) and (b) indicates the presence of a sponge (microemulsion) phase, which becomes anisotropic at later times, (c) and (d). The superposition of slices (c) and (d), namely, the ratio of peaks' positions of  $\sum_{k_z} S(\mathbf{k})$ , is in full agreement with SAXS experimental data for the gyroid mesophase. All quantities are in lattice units.

logarithmic to stretched exponential functions. This confirms the usefulness of our method in apprehending the fundamental phenomenology of amphiphilic fluid mixtures; the presence of transients in these crossovers is gratifying given their experimental observation. In order to rule out an increase in total density as  $x$  is increased as a factor contributing to the slowdown along with the reduction in surface tension, future work should investigate domain growth at constant total density.

The stretched exponential functional form occurring at domain growth-arrested regimes can be ascribed to the accumulation of a large number of relaxation modes associated

with surfactant dynamics onto and at the oil-water interfaces [19]. The late-time structures at these regimes are (a) disordered nonstationary sponge mesophases if the initial amphiphile concentration is lower than a threshold region or (b) well-defined liquid-crystalline cubic gyroid mesophases of pinned domain sizes with defects if this initial concentration is higher than such a threshold. We also found thresholds in the surfactant coupling strengths,  $|g_{ss}|$  and  $|g_{bs}|$ , for a sponge-to-gyroid transition. In the transition region we observed a crossover structure sharing the structural features of both the gyroid and sponge. We also found that, for the number of time steps simulated, both sponge and gyroid exhibit un-

damped oscillations at all length scales. For some length scales, the temporal trend of their Fourier amplitudes is to slowly die out; for others, it increases.

We found that extremely slow domain growth can be mistaken for genuine arrested growth if attention is not paid to minute length scales. Truly segregation-halted regimes exhibit oscillations in average domain size, which can be seen at sufficiently late times. These oscillations are caused partly by Marangoni flows generated by inhomogeneities in the surfactant adsorbed on the oil-water interface, and partly by a surfactant dynamics dictated by competing mechanisms, namely, surfactant attraction towards the interface and surfactant-surfactant interactions. Because our model does not presuppose that all the surfactant is adsorbed on the interface, as Langevin approaches based on the adiabatic approximation do [25,28,59], surfactant-surfactant interactions are not limited to repulsion. Hence, in regimes of large surfactant concentration, and especially in those for which regions of the (oil-water) interface can be sufficiently close to each other, surfactant is not constrained to dwell on the interface; rather, it is reasonable to propose the existence of an adsorption-desorption dynamics driving surfactant towards and away from it. Our results showing that (a) an increase in  $|g_{ss}|$  excites higher frequencies, (b) an increase in  $|g_{bs}|$  dampens most frequencies, and (c) there appear surfactant currents bridging adjacent interfacial regions confirm this proposal.

Our method is not only the first lattice-Boltzmann model to deal with segregation kinetics in three-dimensional amphiphilic fluid mixtures, but the first complex fluid model to unequivocally reproduce the gyroid cubic mesophase, using a high level of abstraction in modeling the amphiphile. The truly mesoscopic, particulate nature of the surfactant in this model accounts for the complex, dynamical behavior observed, even in a noiseless scenario such as ours. It is not surprising that Ginzburg-Landau-based Langevin models which treat surfactant implicitly through a scalar parameter modifying the free energy are only able to exhibit oscillations which decay rapidly in time and whose frequency spectrum has but one peak. Our simulations of liquid-crystalline

mesophases prove that, contrary to what has been previously claimed [59–61], surfactant-surfactant interactions need not be long ranged in order for periodically modulated, long-range ordered structures to self-assemble. In addition, our findings rebut the suggestion [23] that cubic mesophases can be simulated only when the amphiphile is modeled with a high degree of molecular specificity.

The simulation of the sponge and gyroid phases, and their complex oscillatory dynamics, confirms the richness of our model's parameter space. Our lattice-Boltzmann model provides a kinetically and hydrodynamically correct, bottom-up, mesoscale description of the generic behavior of amphiphilic fluids, which is also extremely computationally efficient on massively parallel platforms. Future extensions of this work include the search for regimes leading to equilibrium mesophases of more varied symmetries, the study of shear-induced symmetry transitions, and large-scale studies of defect dynamics in liquid-crystalline phases. In fact, the TeraGyroid project, a successful Grid-based transatlantic endeavor employing more than 6000 processors and 17 teraflops at six supercomputing facilities [63], has its scientific *raison d'être* based on the results we report in this paper. TeraGyroid proves the value of computational steering tools [53] in mapping new parameter space regions of our model.

#### ACKNOWLEDGMENTS

This work was supported by the UK EPSRC under Grant No. GR/M56234 and RealityGrid Grant No. GR/R67699 which provided access to SGI Origin2000 and SGI Origin3800 supercomputers at Computer Services for Academic Research (CSAR), Manchester Computing Consortium, UK. We also thank the Higher Education Funding Council for England (HEFCE) for our on-site 16-node SGI Onyx2 graphical supercomputer. We thank Dr. Rafael Delgado Buscalioni for enlightening discussions and Dr. Keir Novik for technical assistance. N.G.-S. also wishes to thank Professor David Jou, Professor José Casas-Vázquez, and Dr. Juan Camacho at the Universitat Autònoma de Barcelona, Spain, for their support.

- 
- [1] W. M. Gelbart, D. Roux, and A. Ben-Shaul, *Modern Ideas and Problems in Amphiphilic Science* (Springer, Berlin, 1993).
  - [2] D. Chapman and M. N. Jones, *Micelles, Monolayers, and Biomembranes* (Wiley, New York, 1994).
  - [3] *Handbook of Microemulsion Science and Technology*, edited by P. Kumar and K. L. Mittal (Marcel Dekker, New York, 1999).
  - [4] G. Gompper and M. Schick, in *Handbook of Microemulsion Science and Technology*, edited by P. Kumar and K. L. Mittal (Marcel Dekker, New York, 1999).
  - [5] P. Mariani, V. Luzzati, and H. Delacroix, *J. Mol. Biol.* **204**, 165 (1988).
  - [6] S.-J. Marrink and D. P. Tieleman, *J. Am. Chem. Soc.* **123**, 12 383 (2001).
  - [7] V. Luzzati, R. Vargas, P. Mariani, A. Gulik, and H. Delacroix, *J. Mol. Biol.* **229** 540 (1993).
  - [8] G. Gompper and M. Schick, in *Phase Transitions and Critical Phenomena*, edited by C. Domb and J. Lebowitz (Academic Press, London, 1994), Vol. 16, pp. 1–176.
  - [9] N. González-Segredo, M. Nekovee, and P. V. Coveney, *Phys. Rev. E* **67**, 046304 (2003).
  - [10] A. J. Bray, *Adv. Phys.* **43**, 357 (1994).
  - [11] T. Kawakatsu, K. Kawasaki, M. Furusaka, H. Okabayashi, and T. Kanaya, *J. Chem. Phys.* **99**, 8200 (1993).
  - [12] M. Laradji, H. Guo, M. Grant, and M. Zuckermann, *J. Phys. A* **24**, L629 (1991); *J. Phys.: Condens. Matter* **4**, 6715 (1992).
  - [13] A. N. Emerton, P. V. Coveney, and B. M. Boghosian, *Phys. Rev. E* **55**, 708 (1997).
  - [14] J. M. Seddon and R. H. Templer, in *Handbook of Biological Physics*, edited by R. Lipowsky and E. Sackmann (Elsevier Science, London, 1995), Vol. 1, pp. 97–153.
  - [15] P. C. Hohenberg and B. I. Halperin, *Rev. Mod. Phys.* **49**, 435

- (1977).
- [16] B. I. Halperin, P. C. Hohenberg, and S. K. Ma, *Phys. Rev. B* **10**, 139 (1974).
- [17] J. H. Yao and M. Laradji, *Phys. Rev. E* **47**, 2695 (1993).
- [18] M. Laradji, O. G. Mouritsen, S. Toxvaerd, and J. Zuckermann, *Phys. Rev. E* **50**, 1243 (1994).
- [19] F. W. J. Weig, P. V. Coveney, and B. M. Boghosian, *Phys. Rev. E* **56**, 6877 (1997).
- [20] P. J. Love, P. V. Coveney, and B. M. Boghosian, *Phys. Rev. E* **64**, 021503 (2001).
- [21] R. D. Groot and T. J. Madden, *J. Chem. Phys.* **108**, 8713 (1998).
- [22] R. D. Groot, T. J. Madden, and D. J. Tildesley, *J. Chem. Phys.* **110**, 9739 (1999).
- [23] P. Prinsen, P. B. Warren, and M. A. J. Michels, *Phys. Rev. Lett.* **89**, 148302 (2002).
- [24] M. Nekovee and P. V. Coveney, *J. Am. Chem. Soc.* **123**, 12 380 (2001).
- [25] M. Nonomura and T. Ohta, *J. Phys.: Condens. Matter* **13**, 9089 (2001).
- [26] M. Imai, A. Saeki, T. Teramoto, A. Kawaguchi, K. Nakaya, T. Kato, and K. Ito, *J. Chem. Phys.* **115**, 10525 (2001).
- [27] S. Qi and Z.-G. Wang, *Phys. Rev. E* **55**, 1682 (1997).
- [28] G. Gompper and M. Hennes *J. Phys. II* **4**, 1375 (1994).
- [29] G. Gompper and J. Goos, *Phys. Rev. E* **50**, 1325 (1994).
- [30] T. Ohta and K. Kawasaki *Macromolecules* **19**, 2621 (1986).
- [31] A. V. Zvelindovsky, G. J. A. Sevink, and J. G. E. M. Fraaije, *Phys. Rev. E* **62**, R3063 (2000).
- [32] B. A. C. van Vlimmeren, N. M. Maurits, A. V. Zvelindovsky, G. J. A. Sevink, and J. G. E. M. Fraaije, *Macromolecules* **32**, 646 (1999).
- [33] P. V. Coveney, *Philos. Trans. R. Soc. London, Ser. A* **361**, 1057 (2003).
- [34] D. Gueyffier, J. Lie, A. Nadim, R. Scardovelli, and S. Zaleski, *J. Comput. Phys.* **152**, 423 (1999).
- [35] S. Succi, *The Lattice-Boltzmann Equation—For Fluid Dynamics and Beyond* (Oxford University Press, Oxford, 2001).
- [36] H. Chen, B. M. Boghosian, P. V. Coveney, and M. Nekovee, *Proc. R. Soc. London, Ser. A* **456**, 2043 (2000).
- [37] M. Nekovee, P. V. Coveney, H. Chen, and B. M. Boghosian, *Phys. Rev. E* **62**, 8282 (2000).
- [38] A. Lamura and G. Gonnella, *Int. J. Mod. Phys. C* **22**, 1469 (1998); A. Lamura, G. Gonnella, and J. M. Yeomans, *Europhys. Lett.* **45**, 314 (1999).
- [39] O. Theissen, G. Gompper, and D. M. Kroll, *Europhys. Lett.* **22**, 419 (1998); O. Theissen and G. Gompper, *Eur. Phys. J. B* **43**, 91 (1999).
- [40] The scaling with the number of processing elements (PEs) for our LB model's implementation is close to linearity and super-linear on more than 64 PEs on Cray T3E-1200E and SGI Origin 3800 supercomputers, respectively; cf. P. J. Love, M. Nekovee, P. V. Coveney, J. Chin, N. González-Segredo, and J. M. R. Martin, *Comput. Phys. Commun.* **153**, 340 (2003).
- [41] No entropic LB scheme for immiscible fluid mixtures has been reported to date. See I. V. Karlin, A. Ferrante, and H. C. Öttinger, *Europhys. Lett.* **47**, 182 (1999); H. Chen and C. Teixeira, *Comput. Phys. Commun.* **129**, 21 (2000); B. M. Boghosian, J. Yepez, P. V. Coveney, and A. Wagner, *Proc. R. Soc. London, Ser. A* **457**, 717 (2001); B. M. Boghosian, P. J. Love, P. V. Coveney, I. V. Karlin, S. Succi, and J. Yepez, *Phys. Rev. E* **68**, 025103(R) (2003).
- [42] U. Frisch, D. d'Humières, B. Hasslacher, P. Lallemand, Y. Pomeau, and J.-P. Rivet, *Complex Syst.* **1**, 649 (1987).
- [43] X. Shan and H. Chen, *Phys. Rev. E* **47**, 1815 (1993); **49**, 2941 (1994).
- [44] See URL:<http://www.mpi.org/>
- [45] I. Murray, *Lattice Boltzmann Study of Amphiphilic Fluids*, Centre for Computational Science Internal Report, Department of Chemistry, Queen Mary, University of London, 2001.
- [46] J. S. Rowlinson and B. Widom, *The Molecular Theory of Capillarity* (Clarendon Press, Oxford, 1982).
- [47] J. H. Ferziger and H. G. Kaper, *Mathematical Theory of Transport Processes in Gases* (North-Holland, Amsterdam, 1972).
- [48] M. P. Allen and D. J. Tildesley, *Computer Simulations of Liquids* (Clarendon Press, Oxford, 1990).
- [49] J. D. Gunton, M. San Miguel, and P. S. Sahni, in *Phase Transitions and Critical Phenomena*, edited by C. Domb and J. Lebowitz (Academic Press, New York, 1983), Vol. 8.
- [50] G. Gompper, in *Structure and Dynamics of Strongly Interacting Colloids and Supramolecular Aggregates in Solution*, edited by S.-H. Chen, J. S. Huang, and P. Tartaglia (Kluwer Academic, Dordrecht, 1992).
- [51] V. I. Kovalchuk, H. Kamusewitz, D. Vollhardt, and N. M. Kovalchuk, *Phys. Rev. E* **60**, 2029 (1999).
- [52] J. H. Laurer, D. A. Hajduk, J. C. Fung, J. W. Sedat, S. D. Smith, S. M. Gruner, D. A. Agard, and R. J. Spontak, *Macromolecules* **30**, 3938 (1997).
- [53] J. Chin, J. Harting, S. Jha, P. V. Coveney, A. R. Porter, and S. M. Pickles, *Contemp. Phys.* **44**, 417 (2003).
- [54] D. A. Hajduk, P. E. Harper, S. M. Gruner, C. C. Honeker, G. Kim, and E. L. Thomas, *Macromolecules* **27**, 4063 (1994).
- [55] J. Klinowsky, A. L. MacKay, and H. Terrones, *Philos. Trans. R. Soc. London, Ser. A* **354**, 1975 (1996).
- [56] P. Garstecki and R. Hołyst, *J. Chem. Phys.* **115**, 1095 (2001).
- [57] B. Schwarz, G. Mönch, G. Ilgenfritz, and R. Strey, *Langmuir* **16**, 8643 (2000).
- [58] A. M. Squires, R. H. Templer, J. M. Seddon, J. Woenckhaus, R. Winter, S. Finet, and N. Theyencheri, *Langmuir* **18**, 7384 (2002).
- [59] M. Seul and D. Andelman, *Science* **267**, 476 (1995).
- [60] C. Sagui and R. C. Desai, *Phys. Rev. Lett.* **71**, 3995 (1993); C. Sagui and R. C. Desai, *Phys. Rev. E* **49**, 2225 (1994); **52**, 2807 (1995).
- [61] C. Roland and R. C. Desai, *Phys. Rev. B* **42**, 6658 (1990).
- [62] R. G. Larson, *J. Phys. II* **6**, 1441 (1996).
- [63] See, e.g., *TeraGyroid: Grid-based Lattice-Boltzmann Simulations of Defect Dynamics in Amphiphilic Liquid Crystals*, demonstration at the SuperComputing2003 conference, Phoenix (Arizona, USA), 2003, URLs: <http://www.sc-conference.org/sc2003/>, <http://www.RealityGrid.org/teragyroid-index.html>